Finite Element Analysis and Experimentation of an Icosahedron Frame under

Compression

THESIS
SEPTEMBER 2015

Mohammed AlGhofaily, Captain, RSAF

AFIT-ENY-MS-15-S-051

DEPARTMENT OF THE AIR FORCE
AIR UNIVERSITY

AIR FORCE INSTITUTE OF TECHNOLOGY

Wright-Patterson Air Force Base, Ohio

AFIT-ENY-MS-15-S-051

FINITE ELEMENT ANALYSIS AND EXPERIMENTATION OF AN
ICOSAHEDRON UNDER COMPRESSION

THESIS

Presented to the Faculty

Department of Aeronautics and Astronautics

Graduate School of Engineering and Management

Air Force Institute of Technology

Air University

Air Education and Training Command

In Partial Fulfillment of the Requirements for the

Degree of Master of Science in Aeronautical Engineering

Mohammed AlGhofaily

Captain, RSAF

September 2015

DISTRIBUTION STATEMENT A.
APPROVED FOR PUBLIC RELEASE; DISTRIBUTION UNLIMITED.

AFIT-ENY-MS-15-S-051

FINITE ELEMENT ANALYSIS AND EXPERIMENTATION OF AN
ICOSAHEDRON UNDER COMPRESSION

Mohammed AlGhofaily

Captain, RSAF

Committee Membership:

Dr. Anthony Palazotto
Chair

Dr. Marina Ruggles-Wrenn
Member

Lt. Col. Anthony M. Deluca, PhD
Member

AFIT-ENY-MS-15-S-051

Abstract

A nonlinear analysis of a 3D icosahedron frame was conducted using ABAQUS, under a compressive load in which collapse occurs. The frame was created in SolidWorks using the material properties of the 3D plastic building material VeroBlue. Two considerations were made: the computational features of the frame, and the comparison between the experimental solution to the numerical solution. Two studies were also considered in this research: The first study was a comparison between the seven-inch and the four-inch icosahedron model with identical weight to buoyancy ratios; and the second study was a comparison between the seven-inch icosahedrons frame, with the experimental results of the data that was collected. The results of both studies are analyzed to compare against and verify the results of numerical computational model.

iv

Acknowledgments

Table of Contents

List of Figures

x

List of Tables

List of Symbols

Symbol	Description
A	Beam Cross-Sectional Area
AFIT	Air Force Institute of Technology
B	Buoyancy
BC	Boundary Condition
CAD	Computer Aided Design
dt	Time Step
DoF	Degree of Freedom
E	Modulus of Elasticity
ft	Feet
FEA	Finite Element Analysis
FEM	Finite Element Model
g	Acceleration of Gravity
GPa	Gigapascal
in	Inches
I	Area Moment of Inertia
K	Stiffness Matrix
Kg	Kilogram
lb	Pound
L	Beam Length

LTAV	Lighter Than Air Vehicle
m	Meter
MATLAB	Matrix Laboratory
MPa	Megapascal
N	Newton
psi	Pound Per Square Inch
r	Icosahedron Radius
r_{beam}	Beam Radius
V_{frame}	Frame Volume
V_i	Icosahedron Internal Volume
vs	versus
W	Weight
ρ_{air}	Air Density at Seal Level
ρ_{frame}	Frame Density

I. Introduction

1.1 Chapter Overview

The first airships, or dirigibles, were developed in the 1800s [4]. These simple, lighter-than-air vehicles (LTAV) were filled with lifting gas to achieve positive buoyancy in air. Buoyancy is the force exerted on an object by the fluid in which it is submerged. The new development of a LTAV which generates lift by evacuating the air inside of the structure, creating an inner vacuum, had not been researched at that time. This research introduces the development of a numerical model for an evacuated frame in the shape of an icosahedron. The frame supports the external pressure acting on the structure, caused by evacuating the internal gas, which results in a vacuum. The finite element results are then compared to the experiments of the frame under a compressive applied load (where the frame is constructed through the use of 3D printing).

This chapter will describe the objective of this research, and highlight the history of LTAVs, with particular consideration given to why researchers decided upon the icosahedron. The assumptions and methodology used in this thesis will also be presented.

1.2 Objective

The design and manufacture of an icosahedron-shaped frame for a LTAV, to test under compressive load, are of particular interest. The objectives of this research are: to gain a better understanding of the compressive load resistance of an icosahedron frame; design and manufacture the frame using a 3D printer; the experimental technique itself;

and the evaluation and comparison of the finite elements analysis of the plastic material used by the 3D model. An additional objective relates to the weight to buoyancy ratio, which was found by another researcher that it was possible to establish a constant ratio, and vary the size of the structure, including the frame and membrane without variation in the internal stress, which was studied for the frame itself.

To evaluate the structure, a nonlinear finite element analysis (FEA) using the Newton Raphson technique has been used. The Newton Raphson technique is a method to find successively better approximations of the roots of a real valued function [15]. Furthermore, an eigenvalue-eigenvector analysis had been carried out to give a comparison to the nonlinear analysis. The Archimedes principle states the relationship which allows a structure to become lighter-than-air (LTA) is when an object is submerged in any fluid, a buoyant force is expected equal to the weight of the displaced fluid. The FEA will provide the behavior of the response to specific loading conditions which was shown to be nonlinear to the LTAV.

1.3 History of LTAV

An evacuated LTAV is not a new concept; it has been used for decades. The floating air vehicle dates back to the 1600s when an Italian monk, Francesco Lana de Terzi proposed the "Aerial Ship ", and stated:

"The preceding inventions did not exhaust the ardour or the curiosity of the human intellect, but have, rather, spurred it to seek how men could, after the fashion of birds, also fly in the air. No one has; however, deemed it possible to construct a vessel that would travel in air as if it were supported on water. In addition, it has not been thought practicable to make a machine lighter than the air itself, which is necessary first to do in order to accomplish the desired end" [11].

The main idea of the statement is that Terzi wanted to invent objects lighter than air.

The hot air balloon was designed in 1709, and it was the first LTAV [8]. The concept involved heating the air inside the balloon to reduce the density [3]. This principle led to the creation of dirigibles, in which the gas used inside the vessel was comprised of Helium or Hydrogen. Dirigibles were the first air vehicles; and there are three different types of dirigibles: non-rigid, semi-rigid, and rigid. The rigid and non-rigid use a framework to retain the vehicle's shape by use of necessary internal gas. The semi-rigid contains a partial framework to distribute the lifting loads [3]. Dirigibles are not without their own challenges, however, including speed, control limitations, safety, and poor ground handling [10].

Currently, by using modern materials and manufacturing techniques, a vacuum can be created to create positive buoyancy, which results from evacuating the structure. The sphere is an ideal shape for a vacuum LTAV because it achieves the greatest stiffness with the minimum weight, but is difficult to manufacture. This research focuses on an icosahedron structure, which closely resembles a sphere.

1.4 The Icosahedron

The icosahedron shown in figure 1 is a regular polyhedron solid [24]. One of the advantages of the icosahedron is that it is symmetrical, containing 20 equilateral triangles that form the shape. The reason why the bubbles form a shape of a sphere and float, is because it is the ideal geometric arrangement where the weight of the bubble is less than the volume that surrounds it; therefore, the external pressure causes lift. However, if we

3

want to develop a sphere that has an internal vacuum, we have to increase the thickness

of the sphere, thus, increasing the structure's weight. Traditionally, these structures have

been designed with very thick walls to resist buckling. The icosahedron frame can

provide the symmetry, spherical shape, and the necessary structural stiffness and this

result in uniform stress distribution.
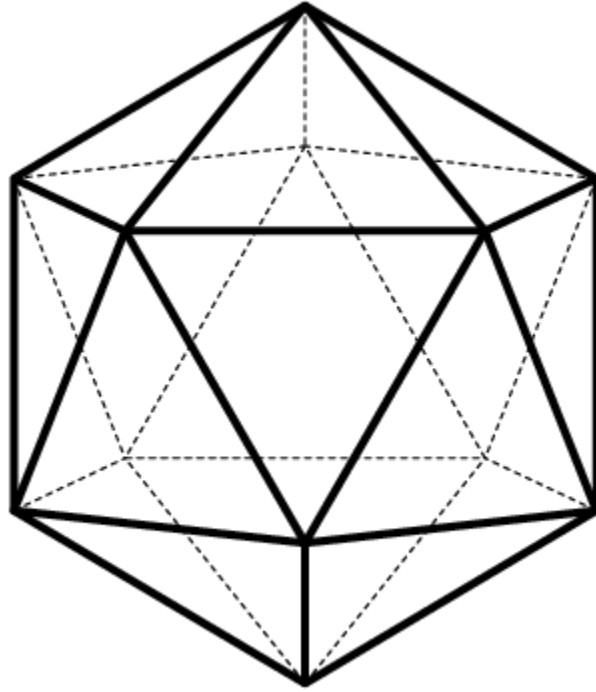
Figure 1: Icosahedron Frame

1.5 Methodology

The FEM makes it easy to study complicated structures, which allow analysis of

structures like the Icosahedron. The computer program ABAQUS is the finite element

tool used in the analysis of the structure.

When a compressive load is applied to the structure, some design challenges result, such as structural instability and integrity. Structural instability is the geometric inability of the structure to maintain equilibrium due to the incapability to resist external work through internal energy [23]. On the other hand, structural integrity is the ability of the structure to resist the external load without internal failure. The geometric shape and material properties of the structure have a relationship with both structural stability and integrity.

1.6 Assumptions and Limitations

FEA includes assumptions and approximations. Following assumptions were used in this research:

1. Structural frame model:

    a. The entire load applied to the skin is distributed to the frame with no moment.

    b. Frame members act like a beam.

2. Manufacturing of the frame

    a. Minimum diameter for the beam is 0.1875 inch.

    b. Maximum diameter for the frame is 7 inch.

1.7 Overview

- Chapter 1: States the objectives of the thesis, the history of LTAVs, the Icosahedron, and the methodology.

- Chapter 2: Summarizes the theory present in the relevant literature related to the structural behavior

- Chapter 3: The methodology of the development of the different models using Finite Elements analysis techniques.

- Chapter 4: Describes and provides the results and the analysis of the Icosahedron models and comparison for different material properties.

- Chapter 5: Provides the research's conclusion and future work recommendations.

II. Theory

2.1 Chapter Overview

This research will explore two main areas: applying compressive load on the top of the icosahedron structure considering the computational features of the frame and comparing a constant weight to buoyancy ratio (W/B) between two frames. This will evaluate the internal stress placed upon the two different frames, while also comparing the experimental solution to the numerical solution. Previous research by Ruben Adorno-Rodriguez and Trent Metlen [18] [22] established a baseline for this research by providing an understanding of the static response of the structure to atmosphere pressure. The purpose of this chapter is to summarize the research which has been carried out to date for the lighter than air vehicle (LTAV), and the behavior of an icosahedron structure. The discussion starts with previous research followed by nonlinear analysis, the buckling and the collapse compressive failure, the manufacture of the frame, and concludes with a summary.

2.2 Previous Research

Ruben Adorno-Rodriguez [18] completed his research concerning an icosahedron frame structure, which was originally developed by Trent T. Metlen's investigation of LTAVs "to become a viable method of transportation" [22]. Archimedes' principle states that a body immersed in a fluid is buoyed up by a force equal to the weight of the displaced fluid [11]. This principle applies to both floating and submerged bodies. It explains not only the buoyancy of ships and other vessels in water, but also the reason behind why a balloon rises in the air, and the apparent loss of weight of objects

underwater. In determining whether a given body will float in a given fluid, both weight and volume must be considered; that is, the relative density, or weight per unit of volume, of the body compared to the fluid determines the buoyant force. If the body is less dense per volume than the fluid, it will float, or in the case of a balloon, it will rise. If the body is more dense than the fluid, it will sink. Relative density also determines the proportion of a floating body that will be submerged in a fluid. If the body is two-thirds as dense as the fluid, then two-thirds of its volume will be submerged, displacing in the process a volume of fluid whose weight is equal to the entire weight of the body. In the case of a submerged body, the apparent weight of the body is equal to its weight in air, less the weight of an equal volume of fluid. Weight to Buoyancy ratio (W/B) is a concept that establishes the buoyancy in a structure with respect to its own weight [18].

In his research, Adorno-Rodriguez determined an equation for selecting a material that will satisfy the weight-to-buoyancy ratio (W/B) necessary to achieve lift. His calculation accounted for the atmospheric effects, and is shown in Equation (1) [18].

$$\frac{W}{B} = \frac{9.5745tr^2\rho_{skin} + 99.098(2c - c^2)r_{beam}^2 r\rho_{frame}}{[2.5362r^3 - V_r](\frac{P_{air,o}}{RT_{air,o}})} + \frac{P_{air,i}T_{air,o}}{P_{air,o}T_{air,i}} \tag{1}$$

Where:

B = buoyancy of the structure

c = beam thickness-to-radius ratio (c=t_{beam}/r_{beam})

$P_{air,i}, P_{air,o}$= inner and outer air pressure, respectively

R= air specific gas constant

r=radius of icosahedron ($0.9511l_{beam}$)

$T_{air,o}, T_{air,i}$= inner and outer air temperature, respectively

W= structure weight

V_r= volume reduction

$\rho_{frame}, \rho_{skin}$= frame and skin densities, respectively

He constructed three different combinations of materials to plot the W/B for seven different models. Figure 2 shows his results for the relationship of the applied pressure to the max von Mises stresses, which is the maximum distortion energy criterion and is often used to estimate the yield of ductile materials [18] [27]. The horizontal lines represent lines of positive buoyancy indicating a threshold, which the applied stress on the structure must exceed for the structure to float in air. The dashes lines represent the yield strength of the material.
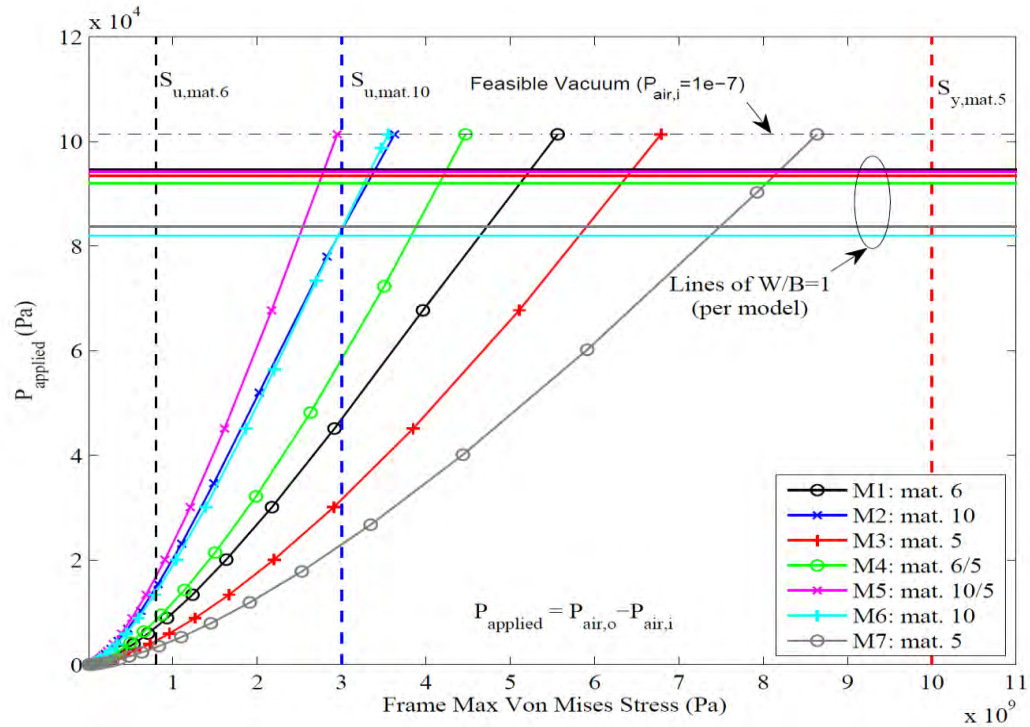
Figure 2: Applied Pressure versus Max Von Mises Stress for the Frame [18]

9

Figure 2 was conducted using a static analysis. The plot shows the frame has significant internal stresses which are above the yield strength of the material, and cannot achieve the required positive buoyancy. However, in this research, the material considered is VeroBlue, which is the material, used in the 3D printer and the focus will be to manufacture the frame and compare the analysis with experimentation. The W/B for only the frame is shown in equation (2).

$$\frac{W}{B} = \frac{V_{frame}\rho_{frame}}{V_{internal}\rho_{air}} \tag{2}$$

Where:

W/B = buoyancy Ratio

ρ_{Frame}, ρ_{air}= density of the frame and air, respectively

$V_{Frame}, V_{internal}$= Volume of the frame and internal volume, respectively.

The icosahedron has equilateral triangular faces and the height of each triangle can be calculated using the Pythagorean Theorem, as follows:
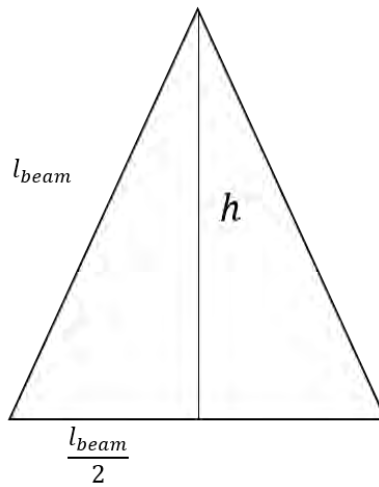
Figure 3: Icosahedron triangle [28]

10

Where:

l_{beam}= Length of the beam

$$h^2 = l_{beam}^2 - (\frac{l_{beam}}{2})^2 \qquad \text{(3) [28]}$$

$$h^2 = (\frac{3}{4}l_{beam})^2 \qquad \text{(4) [28]}$$

$$h = \frac{\sqrt{3}}{2}l_{beam} \qquad \text{(5) [28]}$$

The volume of the icosahedron is represented by 20 triangles of height of r_i, where $r_i = OP$, as shown in Figure 4.
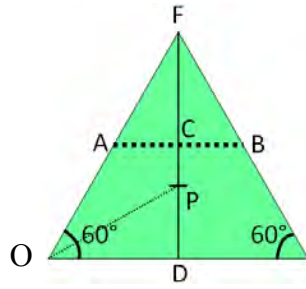
Figure 4: Equilateral Triangle [18]

Knowing the angle between sides is 60° :

$$DP = \frac{l_{beam}}{2}tan30° = \frac{\sqrt{3}}{6}l_{beam} \qquad \text{(6) [18]}$$

$$OC = \frac{l_{beam}}{4}cot18° \qquad \text{(7) [18]}$$

$$OP^2 = OC^2 - CP^2 = OC^2 - (CD - DP)^2 = OC^2 - (\frac{h}{2} - DP)^2 \qquad \text{(8) [18]}$$

11

$$OP^2 = \frac{l_{beam}^2}{16}\cot^2 18° - \left(\frac{\sqrt{3}}{4}l_{beam} - \frac{\sqrt{3}}{6}l_{beam}\right)^2 = l_{beam}^2\left(\frac{\cot^2 18°}{16} - \frac{1}{48}\right) \qquad \text{(9) [18]}$$

$$r_{i=}OP = l_{beam}\sqrt{\frac{\cot^2}{16} - \frac{1}{48}} \approx 0.7558 l_{beam} \qquad \text{(10) [18]}$$

Where the area and the internal volume is shown in equation 11 and 12

$$A = \frac{\sqrt{3}}{4}l_{beam}^2 \qquad \text{(11) [18]}$$

$$V_i = 20[\left(\frac{1}{3}A\right)r_i] = \frac{5}{12}(3 + \sqrt{5})l_{beam}^3 \qquad \text{(12) [18]}$$

The volume of the frame with 30 beams are shown in equation 13

$$V_f = 30\pi r_{beam}l_{beam} \qquad \text{(13) [18]}$$

Where:

r_{beam}= Radius of the beam

Then combining the equation 2, 12 and 13 we get the equation for the radius of the beam

$$r_{beam} = r\sqrt{\frac{(\frac{W}{B})\rho_{air}}{39.0742\rho_{frame}}} \qquad (14)\ [18]$$

Where:

r= Radius of icosahedron frame

2.3 Nonlinear Analysis

The nonlinear analysis analyzes the behavior of the structure and it is a byproduct its stiffness. The term "stiffness" can be used to define the difference between the nonlinear and linear structural behavior. In a linear structure analysis, the amount of force per unit displacement is only dependent upon material and geometric properties of the structure. In a nonlinear geometric analysis, the stiffness is related not only to the material and geometric properties of the structure but also to the structure's displacements characteristic; it can be presented by equation (15) in which the linear matrix is $\lfloor K_{ij} \rfloor$ and the nonlinear matrix $\lfloor \widetilde{K}ij \rfloor$ which has the displacement function incorporated [16].

$$\lfloor \widetilde{K}ij \rfloor \{D_j\} = \{F_i\}$$
$$\lfloor \widetilde{K}ij \rfloor = \lfloor K_{ij} \rfloor + [\varDelta K_{ij}(u)] \qquad (15)$$

13

Where:

K= stiffness

F= force

D= Displacement

For linear structures, if the stiffness is represented in a simple form (k=F/D), then for a nonlinearly responding structure, this form must be modified. In this research, we look at this type of response [16]. In geometric nonlinearly, the nonlinearity is constantly changing. In a linear scenario the stiffness k is equal to applied force per unit displacement.

In a nonlinear analysis, the stiffness is equal to the rate of change of force per displacement thus ($k = dP/dD$). The Newton Raphson technique is the most common nonlinear solution [15], which will be discussed in the following section.

2.2.1 Newton Raphson Technique

The Newton Raphson technique is a method to find successively better approximations of the roots for real value function [15]. It is used to solve the nonlinear equation. The nonlinear static equilibrium equations is

$$K_T \Delta q = -F(q)$$

(16)

$$[K + N_1(q) + N_2(q^2)]\Delta q = -\left[K + \frac{1}{2}N_1(q) + \frac{1}{3}N_2(q^2)\right]q + R$$

(17)

Where:

K= linear stiffness matrix

K_T= tangent stiffness matrix

N_1= linear function of q

N_2= quadratic function of q

q= nodal displacement vector

R= nodal loading vector

The Newton Raphson algorithm has the iteration until the residual force vector ΔR becomes sufficiently small until the equilibrium equations are satisfied. This process is repeated until it reaches convergence. Figure 5 shows point A and B, which represent the solution for load increment [16].
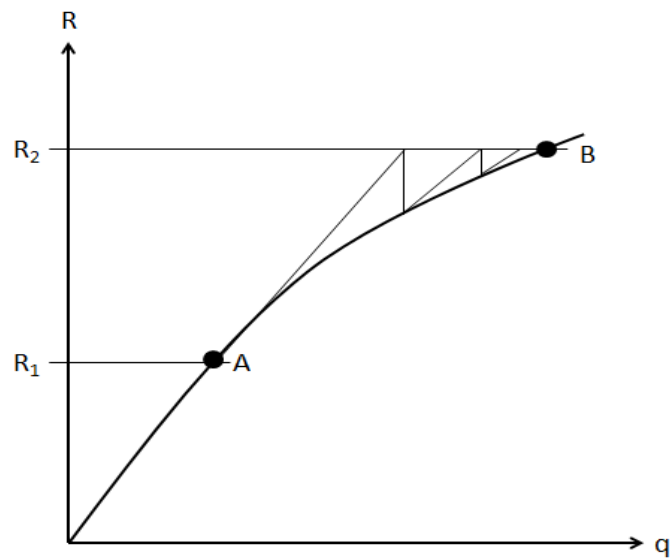
Figure 5: Newton Raphson Algorithm [18]

2.3 Buckling and collapse failure

Buckling and collapse are both related to the structure's geometric design. The difference between them is collapse is characterized by a total nonlinear analysis. All failure modes are related to the structure's stiffness [19].

2.3.1 Buckling failure

Buckling occurs when the structure cannot recover from its initial state of equilibrium after being disturbed. The state of equilibrium is when the structure is able to move back to equilibrium [19]. This is called bifurcation loading, shown in Figure 6,
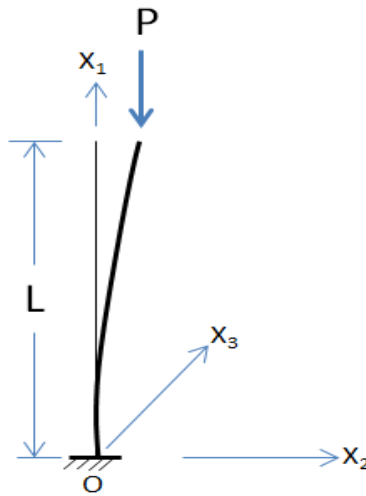
Figure 6: Fixed end column [18]

The force applied to the top end causes a moment at point O, which will cause the column to bend. The stiffness will try to restore the column to its equilibrium state. When the load is increased, it will reach a point when the stiffness cannot restore the structure to the equilibrium state which makes the structure unstable. At this point, the

column has buckled, and the load becomes the critical load. The critical bifurcation load

is represented by equation (18) as shown in Figure 6 [19][2].

$$P = \frac{\pi^2 EI}{4L^2}$$

(18)

Where:

I=area moment of inertia

L=column Length

P= critical load

A linear bifurcation analysis is a process that estimates the eigenvalue, which

represent the critical (bifurcation) loads. This research only analyze the linear bifurcation

analysis to estimate the mode shapes of the structure, to visualize the possible collapse

mode's shapes. The point when the analysis creates the nonlinear response, yielding a

maximum value without bifurcation, is called collapse.

2.3.2 Collapse Failure

Collapse occurs when the structure is not capable of carrying its load. At this

point the structure is globally unstable. When the applied force produces reduction in

stiffness, and the structure can no longer resist this load in equilibrium, the collapsed

mode is introduced [6].

The structure considered becomes vulnerable to collapse when the pressure is

transferred from the skin to the frame. Each member of the frame is subjected to axial

load and transverse load. In this research, the beam is a solid circular member as shown
in Figure 7.
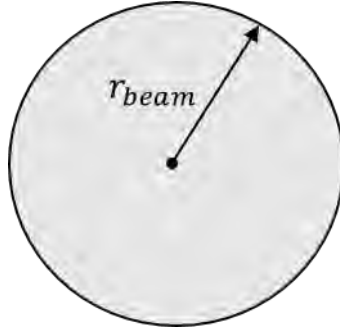
Figure 7: Beam cross-section for icosahedron frame

2.4 Manufacturing the frame

To manufacture the frame, the 3D printer is used as shown in Figure 8. 3D
printing or additive manufacturing is a process of making three-dimensional solid objects
from a digital file [25]. The creation of a 3D printed object is achieved using additive
processes. In an additive process, an object is created by laying down successive layers of
material until the entire object is created. Each of these layers can be seen as a thinly
sliced horizontal cross-section of the eventual object [17]. The object is created using a
virtual design. The virtual design is made in a SolidWorks Program in a type of CAD file
(Computer Aided Design) [20].

To prepare a digital file for printing, the 3D modeling software "slices" the final
model into hundreds or thousands of horizontal layers. When the file is uploaded in a 3D
printer, the object can then be created layer by "sliced" layer. The 3D printer reads every

slice (or 2D image) and creates the object, blending each layer with hardly any visible

sign of the layers, resulting in the three-dimensional object [24] [21].

Figure 8: 3D printer

There are seven processes to print a 3D model [26]:

1. Vat Photopolymerisation

2. Material Jetting

3. Binder Jetting

4. Material Extrusion

5. Powder Bed Fusion

6. Sheet Lamination

7. Directed Energy Deposition

We will only focus on the material Jetting.

Material Jetting is a process applied in droplets through a small diameter nozzle, similar to the way a common inkjet paper printer works, but it is applied layer-by-layer to a build platform making a 3D object and then hardened by ultra violet (UV) light as shown in Figure 9 [26].
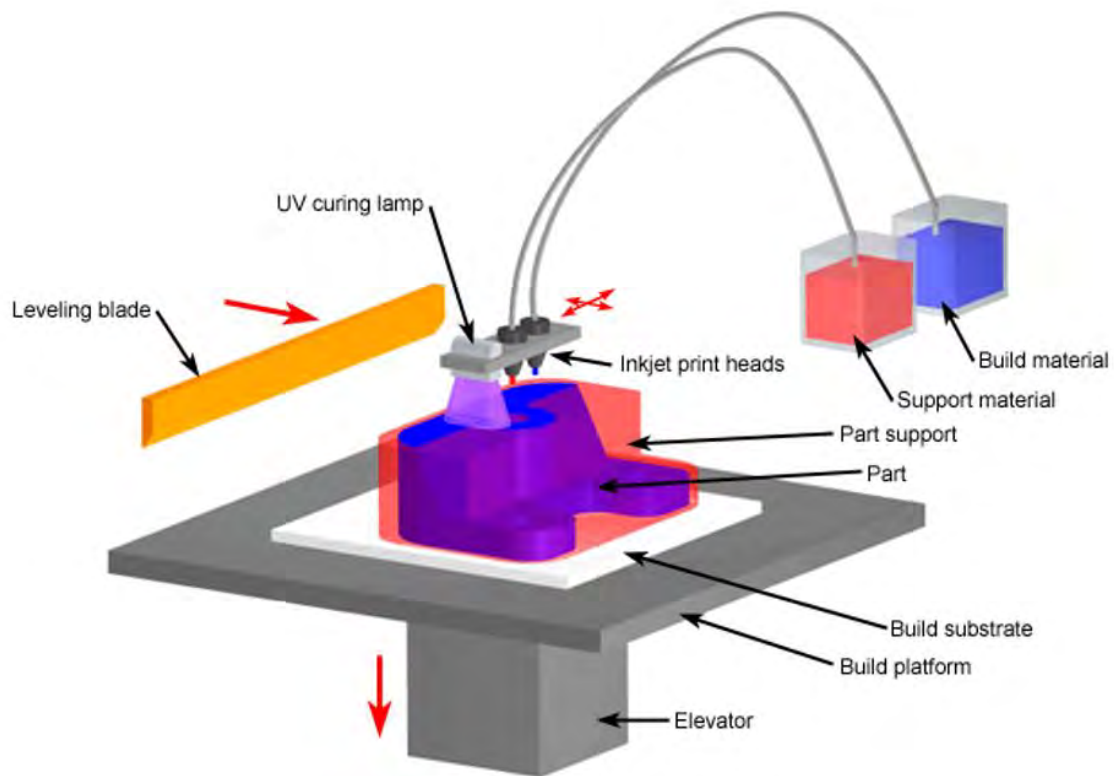
Figure 9: Material-Jetting schematics [23]

With some of the model materials, the 3D printer also jets a gel-like support material for overhangs and complex geometries. This support material is easily removed by hand and with water pressure.
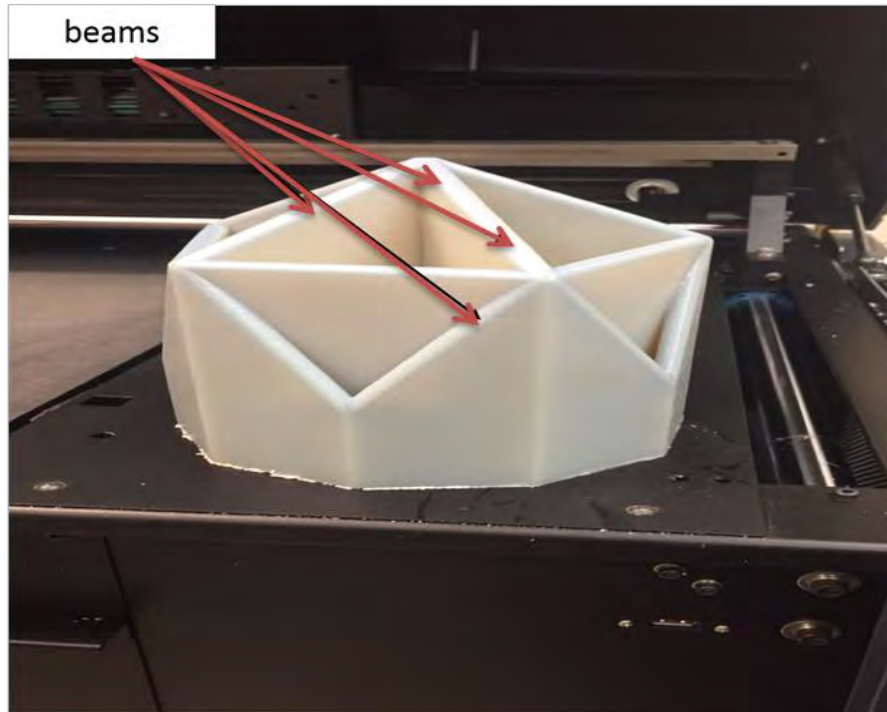
Figure 10: Icosahedron frame with support material
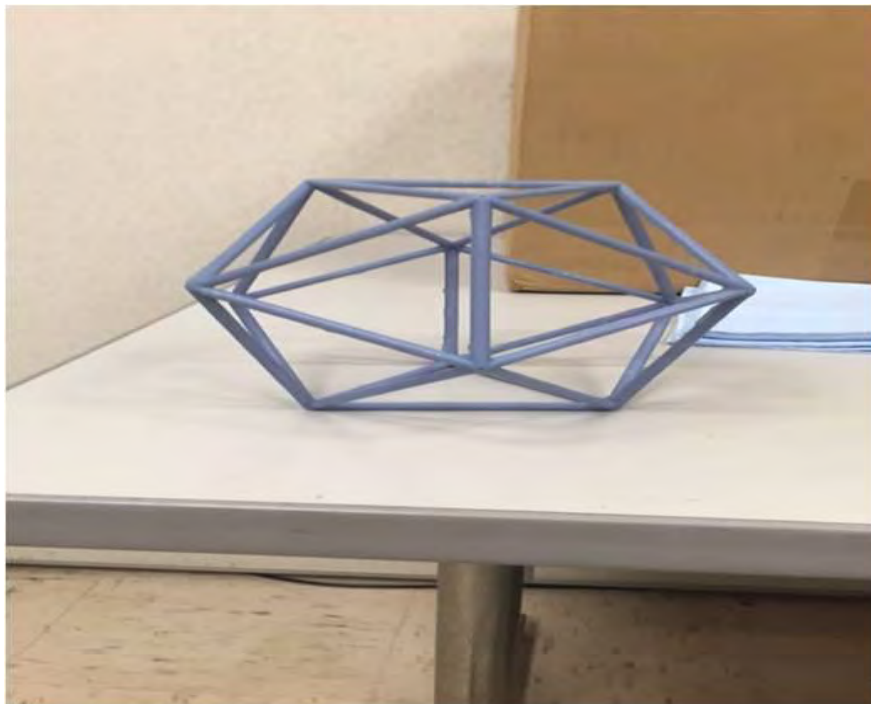
Figure 11: Icosahedron frame after cleaning the support material

21

The Objet500 Connex3 3D printer is used to print the frame. The tray of this printer is 19.7 × 15.7 × 7.9 in. It can build multiple materials with multiple colors and good surface finish. VeroBlue comes from PolyJet's family of rigid photopolymers that provide excellent detail, visualization, durability, and strength [21].

In this research, two studies of material properties were considered. Boston University created a dog bone and generated stress-strain diagrams [13]. This study is very close to the manufacture value, which is reported by Objet [17].The second study shows the values for tensile stiffness being lower than what is reported by Objet [12]. Virginia Tech investigated the VeroWhite material and the changes in part tensile strength and tensile modulus due to changes in orientation and part spacing [12]. VeroWhite has very similar properties to VeroBlue.

Boston University did a study of this material. Their study is to investigate the properties of plastics within prototyping. They created two-dog bone made of VeroBlue plastic and generated a Stress-Strain Diagrams, representing the physical properties of the material [13].

Figure 12: VeroBlue dog bone [13]
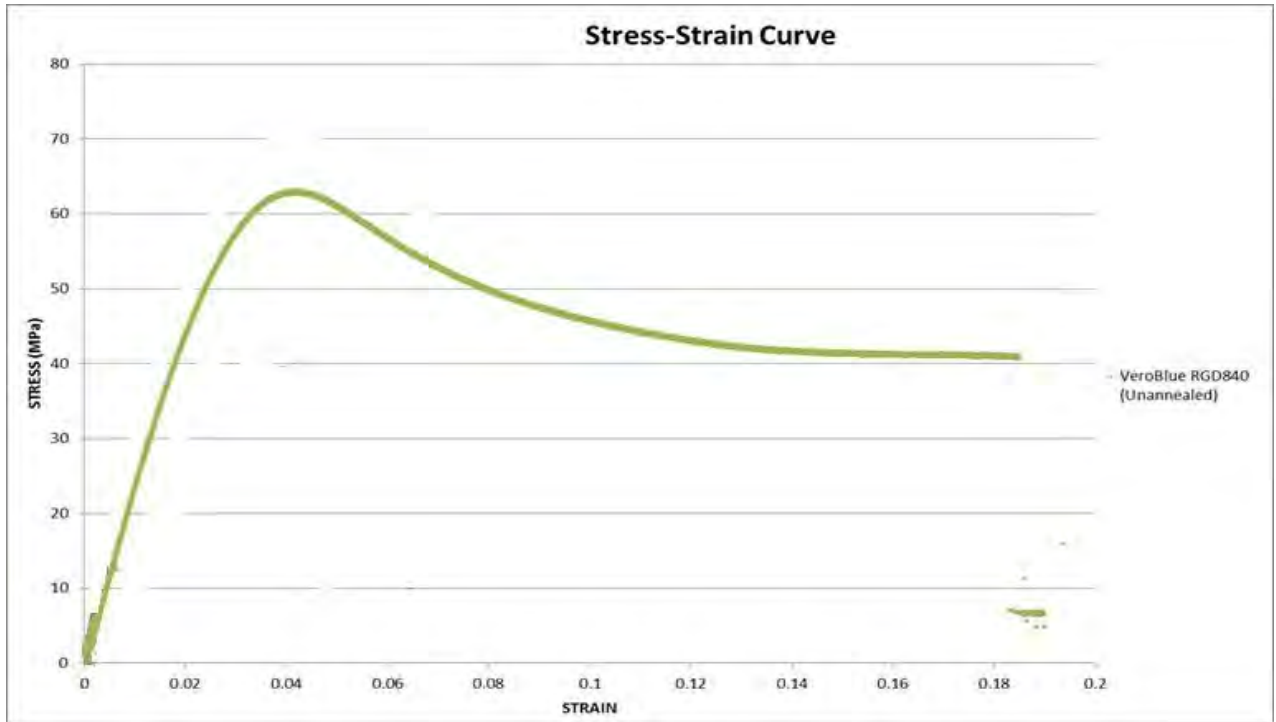
Figure 13: Stress-Strain Diagrams [13]

Table 1: Physical properties of VeroBlue [13]

Elastic Modulus	Yield Strength	Ultimate Tensile Strength
2.29 GPa 3.3e5 psi	50 MPa 7252 psi	63 MPa 9137 psi

On the other hand, Virginia Tech [12] investigated the changes in a part's tensile strength and tensile modulus due to changes in X-Y orientation, Z-orientation, and the part's spacing in the X-Y plane, which is more applicable to the experimental results of this thesis due to the space inside the icosahedron. They then analyzed the specimens'

tensile strength and tensile modulus, using a scientific method approach, based on three parameters: the in-build plane part orientation (X-Y), the out-of-build plane part orientation (Z), and the distance between specimens [12]. The results show that the spacing has the largest effects on tensile strength. This study is used as a guide to compare to the experimental results in this research. They created an Ishikawa Diagram, which is the potential factor which could produce deviation in the mechanical properties of the VeroWhite material as shown in Figure 14 (Cause-and-Effect / Fishbone Diagram) [12].
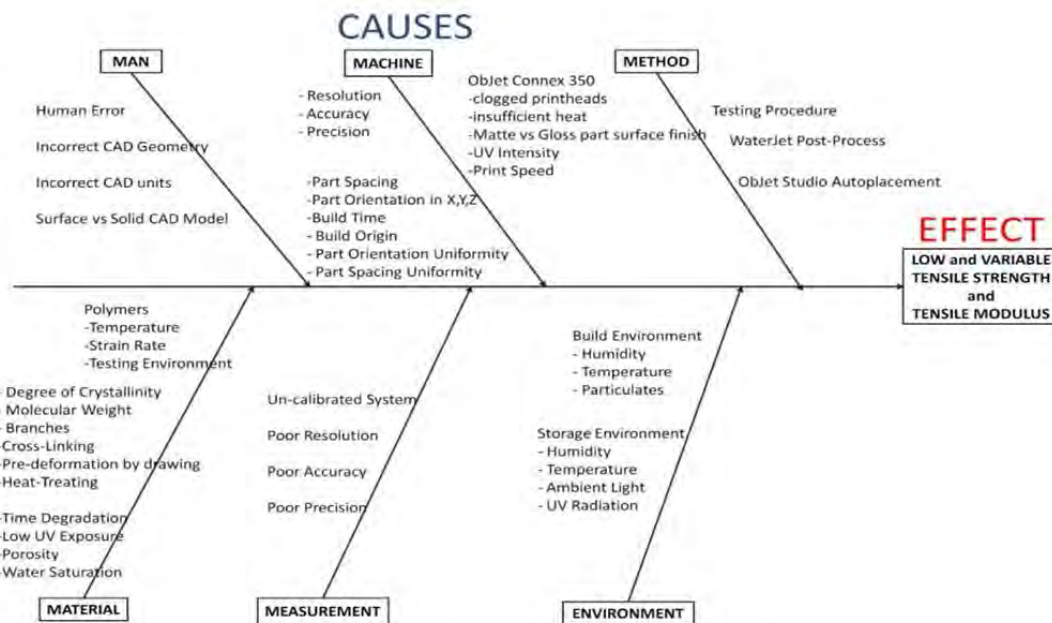
Figure 14: Ishikawa Diagram for PJD-3DP Process [12]

The diagram explains the potential factors that can cause the low and variable tensile strength and tensile modulus of the VeroWhite material. Some causes include: incorrect geometry, 3D printing, methods used to print the object, and environmental differences.

24

Virginia Tech analyzed three parameters X-Y Orientation, Z Orientation, and Part Spacing as shown in figure 15.
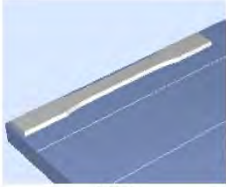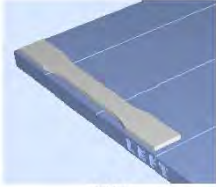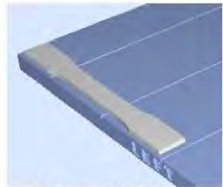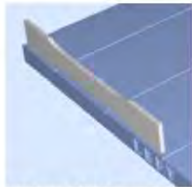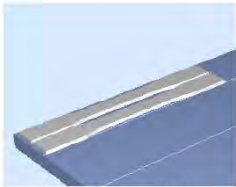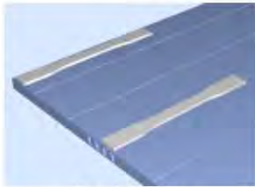
Parameter: X-Y Orientation

XY

Description: The in-plane build orientation of the part such that its length is parallel or perpendicular with respect to the front of the build tray.

YX

Hypothesis: Orienting parts across print-head paths, may lead to lower mechanical properties due to banding from discretized jetting nozzles.

Parameter: Z-Orientation

YX or XY (flat)

Description: The build direction orientation of the part such that the width, not the length, lays flat or angled with respect to the X-Y plane.

YZ or XZ (angled)

Hypothesis: An increase in the number of layers causes curing "print-through" and thus increased mechanical properties for parts with widths aligned in the Z plane (as noted for SL in [17]).

Parameter: Part Spacing

Tight Spacing

Description: The overall spacing between parts in X-Y plane of the build-tray.

Far Spacing

Hypothesis: Smaller spacing may lead to increased mechanical properties due to potential UV over-cure effect.

Figure 15: Experimental Parameters [12]

The researchers printed eight build trays. Five specimens were printed per build tray, with each build tray corresponding to a specific experiment with uniform orientation among all printed specimens [12]. Tensile tests were then conducted, with the results shown in Table 2 and Figure 16 for mean tensile strength and modulus [12].

25

Table 2: Mean Experimental Data [12]

Experiment	Mass (g)	Thickness (mm)	Width (mm)	Tensile Strength (MPa)	Tensile Modulus (MPa)
YXT	10.1	3.23	13.4	32.3	1501
YXF	10.1	3.23	13.4	26.0	1577
YZT	10.5	3.59	13.0	31.2	1696
YZF	10.1	3.43	13.0	24.2	1176
XYT	10.0	3.25	13.4	35.3	1665
XYF	10.0	3.22	13.3	29.0	1719
XZT	10.8	3.66	13.0	37.8	1874
XZF	10.4	3.56	13.0	22.9	1284

The first two letters represent the orientation, and the third letter represent for Part

Spacing (T and F for tight and far spacing, respectively).
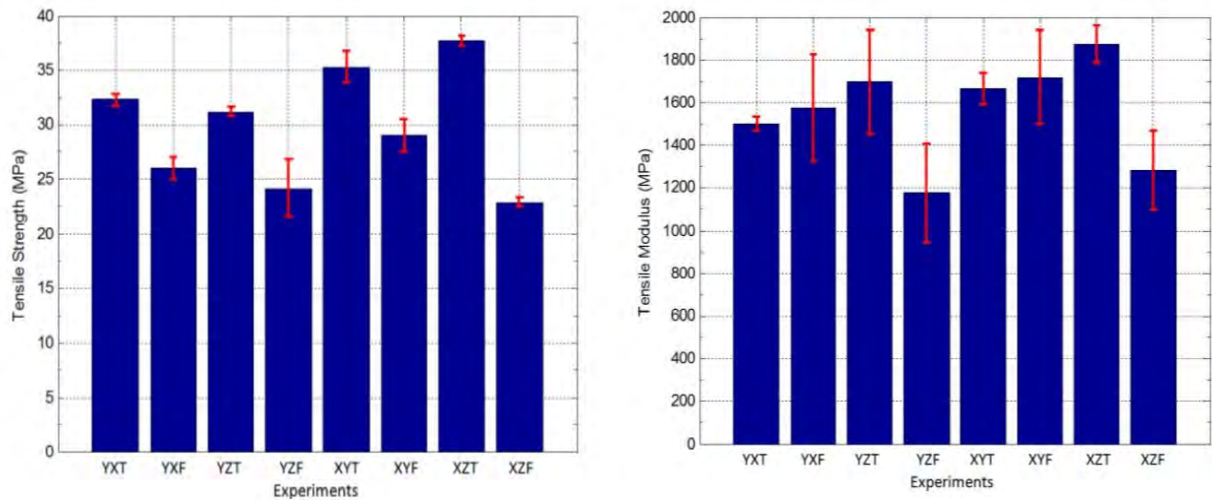
Figure 16: Mean tensile Strentgh (left) , Mean tensile modulus (right) [12]

Considering the design of the icosahedron, it has beams at various angles and the spacing between these beams are significantly large in dimension, the most logical distribution of the modulus and the tensile strength will fall in line with YZF or XZF. This conclusion will be verified when the comparison between the FE model and the experiment is discuss.

2.5 Summary

Nonlinear analysis can solve the complicated mathematical problems. One of the most common methods to solve these is the Newton Raphson technique. There are some considerations necessary when evaluating the structure. Collapse is when the structure cannot carry any additional load, thus, nonlinear analysis will be a main numerical consideration. In addition, the frame used in this research is manufactured using the 3D printer. Also, two material properties studies are being considered, with experimentation being carried out to verify the analysis.

III. Methodology

3.1 Overview

To gain a better understanding of a compressive load carried by an icosahedron, it is necessary to trace the computational features of the frame, and creation of the frame model is required. Metlen and Adorno-Rodriguez created a frame model capable of producing important information about the static response of the icosahedron [22] [18]. This chapter discusses the process used to run the studies and analysis, model development, and the experimental test setup that is used in this research.

3.2 Design of the Frame

The reason for comparing the two different size frames with equal (W/B) ratio was to determine if the internal stress levels were similar in each. Adorno-Rodriguez developed the icosahedron model, and it was the baseline for this research [18]. Figure 17 shows the icosahedron frame model used in ABAQUS. Two icosahedrons have been designed, a seven-inch diameter, and a four-inch diameter. For an initial study with the goal of seeing if an equal (W/B) can produce a similar stress field between frames. Two material properties for VeroBlue are used for this research. One study is to compare a seven-inch icosahedron with a four-inch icosahedron with the same weight-to-buoyancy ratio (W/B) [13]. The second study is to compare the physically constructed seven-inch icosahedron frame from a 3D printed model tested, with the FE model.

First, let us discuss the comparison of two frames that have equal (W/B) using a material utilized in the 3D printer called VeroBlue. The dimensions, as well as the set of

28

material properties for VeroBlue studied in this case, are listed in Table 3 and 4. The finite element model was created with a weight-to-buoyancy ratio of equal magnitude, utilizing Equation (2). The radius of the beam for the seven-inch frame was chosen based on the minimum beam dimension the 3D printer can process; less than that may break the frame due to the water jet used to clean the support material (Figure 18).
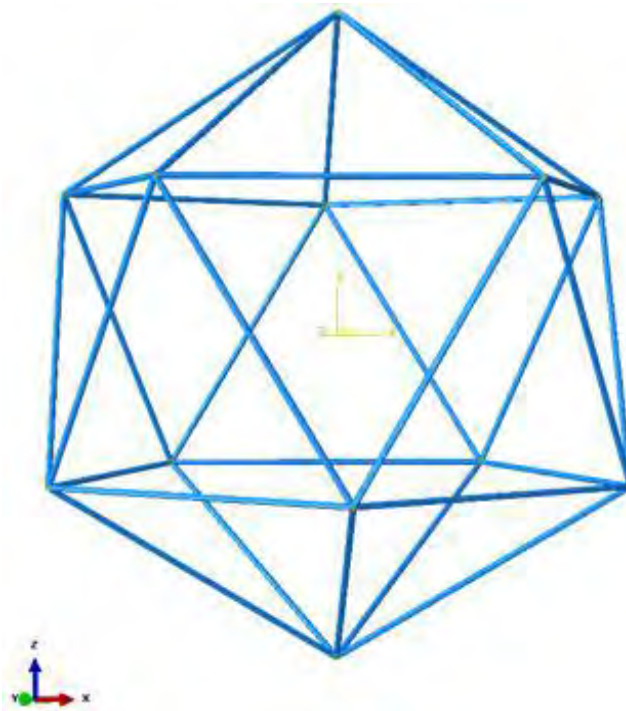
Figure 17: Icosahedron Frame

Figure 18: Water jet cleaning off the support material

Table 3: Icosahedron seven-inch diameter

	Dimension	Units
Diameter (vertex to vertex)	0.1778 (7)	m (in)
Beam cross section Radius	0.00238125 (0.0937)	m (in)
Length of the beam	0.09144 (3.6)	M (in)
VeroBlue Density	1190	kg/m^3
VeroBlue Modulus of Elasticy	2.2945	GPa
VeroBlue Poisson's Ratio	0.35	Unit less

For the four-inch icosahedron, the cross section of the beam is calculated using the same W/B for the seven-inch model. Using equation (2), (12) and (13) to calculate the W/B,

$$\frac{W}{B} = \frac{V_{frame}\rho_{frame}}{V_{internal}\rho_{air}}$$ (2)

Where

$V_{Frame}, V_{internal}$ = Volume of the frame and internal volume, respectively.

$$V_f = 30\pi r_{beam} l_{beam}$$ (13) [18]

$$V_f = 30\pi(0.00238125)(0.09144) = 4.887x10^{-5}m^3$$

$$V_i = \frac{5}{12}(3 + \sqrt{5})l_{beam}^3$$ (12)

$$V_i = \frac{5}{12}(3 + \sqrt{5})0.09144^3 = 1.668x10^{-3}m^3$$

$$\frac{W}{B} = \frac{4.887x10^{-5}1190}{1.668x10^{-3}1.225} = 28.46$$

Then, using this result for the radius, the beam can be formed using equation 5

$$r_{beam} = r\sqrt{\frac{(\frac{W}{B})\rho_{air}}{39.0742\rho_{frame}}}$$ (14) [18]

$$r_{beam} = 0.0508\sqrt{\frac{(28.46)(1.225)}{39.0742(1190)}} = 0.001391 \, m \, ,$$

Where $\rho_{air} = 1.255 \, kg/m^3$

Table 4: Icosahedron four-inch diameter

	Dimension	Units
Diameter (vertex to vertex)	0.1016 (4)	m (in)
Beam cross section Radius	0.001391 (0.0547)	m (in)
Length of the beam	0.05232 (2.06)	m (in)
VeroBlue Density	1190	kg/m^3
VeroBlue Modulus of Elasticy	2.2945	GPa
VeroBlue Poisson's Ratio	0.35	Unit less

Using the Adorno-Rodriguez finite element convergence study, the beams were constructed with B32 beam elements [18]. B32 beams in ABAQUS are Timoshenko beams that allow for transverse shear deformation, and use a quadratic interpolation between nodes [7]. The number of elements used in this analysis was 540 elements.

3.3 Analysis Techniques

The nonlinear problem with large displacement is to be considered for the analysis. In this research, the Newton Raphson technique is used, which was described in the previous chapter. In ABAQUS, the processor starts with initial load increments and the algorithm changes with the initial load increment by 25-75% every time for up to five iterations [18].

During the process, three parameters are changed. These changes are amount of maximum iterations per load increment (10000 increments), the percentage of increment change per iteration, and the amount of equilibrium calculations made before moving onto another iteration (the initial increment size was 1E-05, with a minimum of 1E-036 and a maximum of 0.01). The automatic stabilization, usually incorporated when a membrane is part of the structure is not necessary for this analysis. For further comparison, eigenvalue-eigenvector analyses had been carried out.

3.3.1 Modeling techniques

In this research, nonlinear static analysis is conducted. The nonlinear static analysis is a procedure that solves for the increment equilibrium of a structure given the applied loads [18]. The following modeling techniques and properties are shared in all icosahedron models considered for analysis:

- Dimensionality: Two icosahedrons models - The first is a seven-inch diameter, with a beam radius equal to 0.0937 inches. The second is a four-inch diameter with a beam radius equal to 0.001391 inches, derived from the same W/B of the seven-inch model, using equations (2), (12), (13) and (14), respectively.

- Load: The load, divided by three, is applied at the top of the three vertices, as shown in figure 19. The load was applied until it reached the collapse mode. The seven-inch model had a load of 720 N applied, and the four-inch model had a load of 255 N applied (The total load could easily be applied at a reference point within ABAQUS).

33

- Boundary Conditions: Two boundary conditions (BC) are considered. In the first, at the bottom of frame, the three vertices are fixed as shown in Figure 20. Only three of the degrees of freedom (DOF) are constrained: U1=U2=U3=0. The second is at the top where only two DOFs are constrained: U1=U2=0, allowing the vertical movement as shown in Figure 21 (by the way, these boundary conditions were verified in the experiment since the beams attached to the frames vertices rotated).

- Mesh: the mesh was composed of B32 beam elements for the frame.

- Analysis: the Newton Raphson technique was selected along with asymmetric matrix storage to improve the convergence history [7]. A linear buckling analysis was conducted in one of the models in order to visualize buckling mode shapes.

Adorno-Rodriguez generated the Python code with a MATLAB code. The MATLAB code was modified to change the dimension. All MATLAB codes and Python codes are included in Appendix A and Appendix B, respectively.
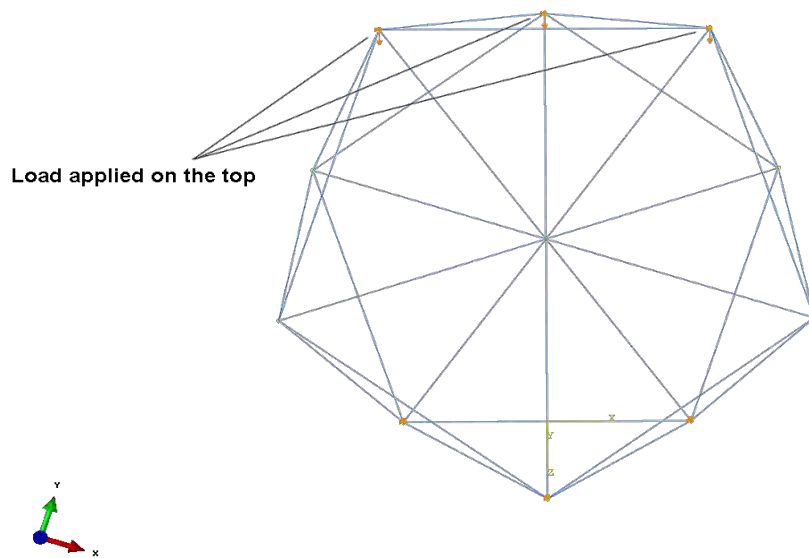
Figure 19: Applied Load at the top
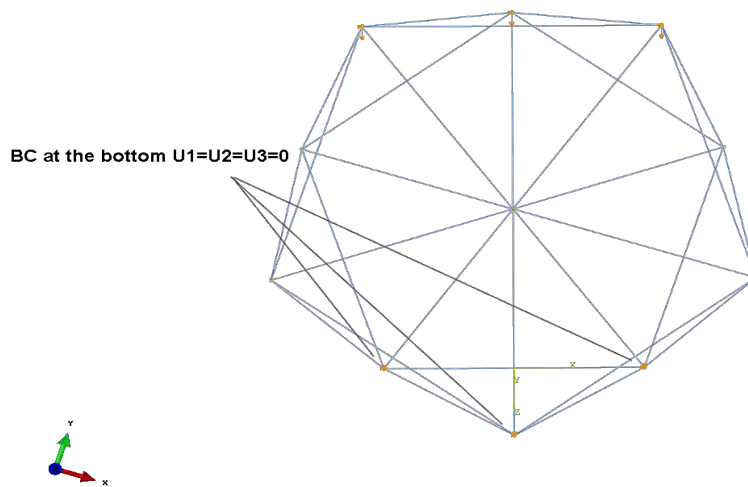
Figure 20: BC at the bottom
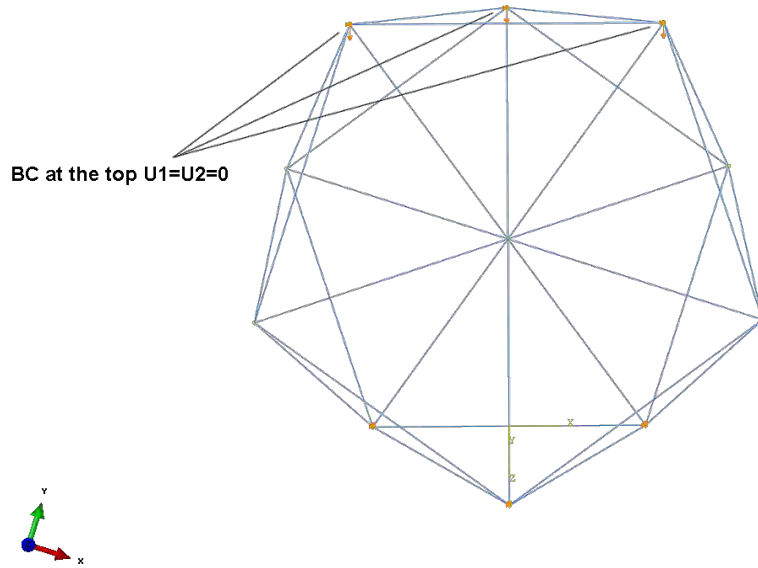
Figure 21: BC at the top

The second study is to compare an equivalent seven-inch icosahedron to the experimental test. The 3D printer model is larger than the original design, due to imperfection in the printer. The new diameter is 7.2 inches, as shown in Figure 22, and the cross section of the beam varied due to the manufacturing uncertainty. In order to develop an average beam dimension, three diameter measurements along the length were taken for each beam, and the final cross section diameter is the average of the thirty beams (shown in Table 5).
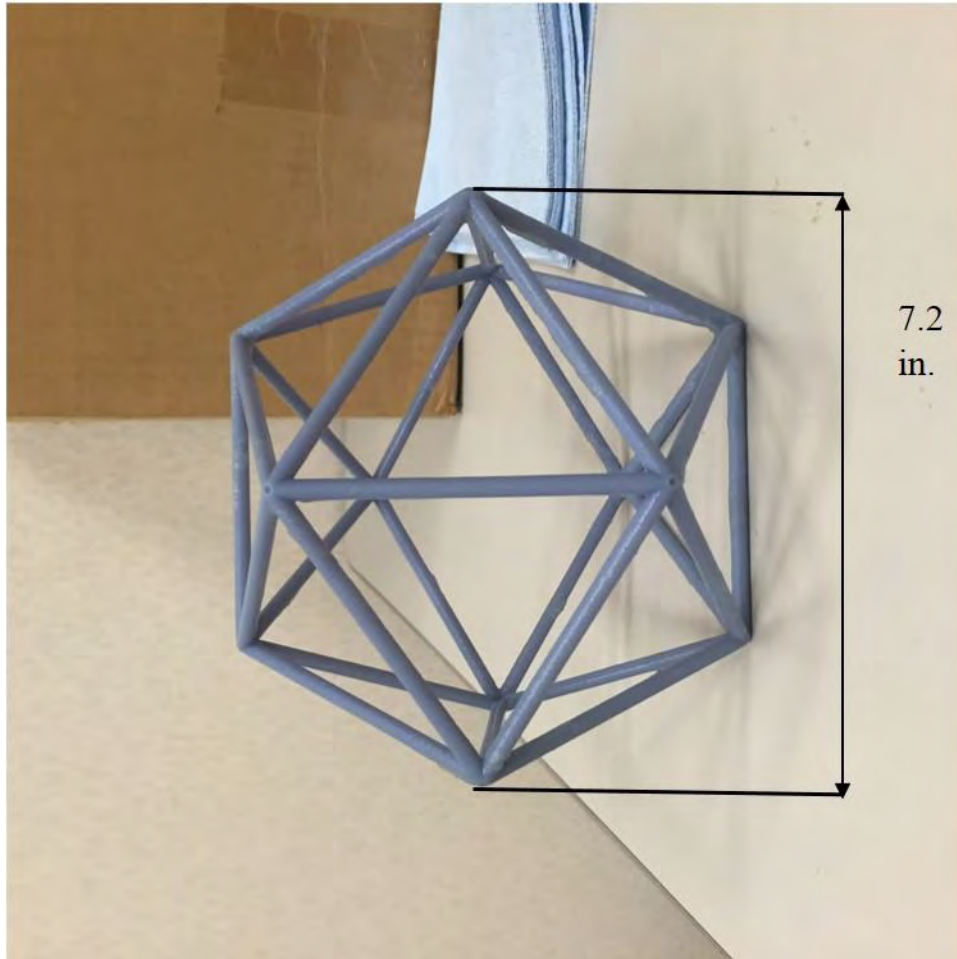
Figure 22: The new dimension for 3D model

Table 5: Beam cross section diameter

	Beam cross section variation diameter (in)			Average diameter in (m)
1	0.186	0.188	0.188	0.187 (0.004758)
2	0.190	0.188	0.186	0.188 (0.004775)
3	0.187	0.187	0.190	0.188 (0.004775)
4	0.190	0.189	0.187	0.189 (0.004792)
5	0.189	0.189	0.190	0.189 (0.004809)
6	0.186	0.187	0.187	0.187 (0.004741)
7	0.189	0.186	0.187	0.187 (0.004758)
8	0.186	0.186	0.186	0.186 (0.004724)
9	0.187	0.186	0.187	0.187 (0.004741)
10	0.186	0.187	0.187	0.187 (0.004741)
11	0.185	0.185	0.185	0.185 (0.004699)
12	0.185	0.186	0.189	0.187 (0.004741)
13	0.185	0.185	0.185	0.185 (0.004699)
14	0.186	0.187	0.187	0.187 (0.004741)
15	0.186	0.186	0.186	0.186 (0.004724)
16	0.187	0.187	0.187	0.187 (0.004750)
17	0.185	0.185	0.185	0.185 (0.004699)
18	0.186	0.186	0.186	0.186 (0.004724)
19	0.187	0.187	0186	0.187 (0.004741)
20	0.185	0.185	0.185	0.185 (0.004699)
21	0.187	0.187	0.186	0.187 (0.004741)
22	0.189	0.185	0.186	0.187 (0.004741)
23	0.187	0.186	0.187	0.187 (0.004741)
24	0.189	0.190	0.189	0.189 (0.004809)
25	0.186	0.186	0.186	0.186 (0.004724)
26	0.187	0.186	0.187	0.187 (0.004741)
27	0.190	0.189	0.187	0.189 (0.004792)
28	0.187	0.186	0.187	0.187 (0.004741)
29	0.185	0.186	0.189	0.187 (0.004741)
30	0.187	0.187	0.187	0.187 (0.004750)
				0.187 (0.004742)

3.4 Experimental Test Setup

A compressive test was performed using the MTS Systems Corporation model 810 Material Test System servo-hydraulic load frame, equipped with: 15kN (3.3 kip) capacity MTS model 661.19E-03. The MTS FlexTest 40 digital controller with MTS FlexTest 40 Station Manager and MultiPurpose TestWare (MPT) application was used for the input signal and data collection. Linear Variable Differential Transformer (LVDT) model LBB-315-PA-100-1, was used to verify the accuracy of the displacement measurements of the MTS machine. The MTS machines have grips, not a flat surface for the placement of the frame. Thus, the manufacturing of a fixture was required in order to place the frame in flat platform. The testing station is pictured in Figure 23 to 25.
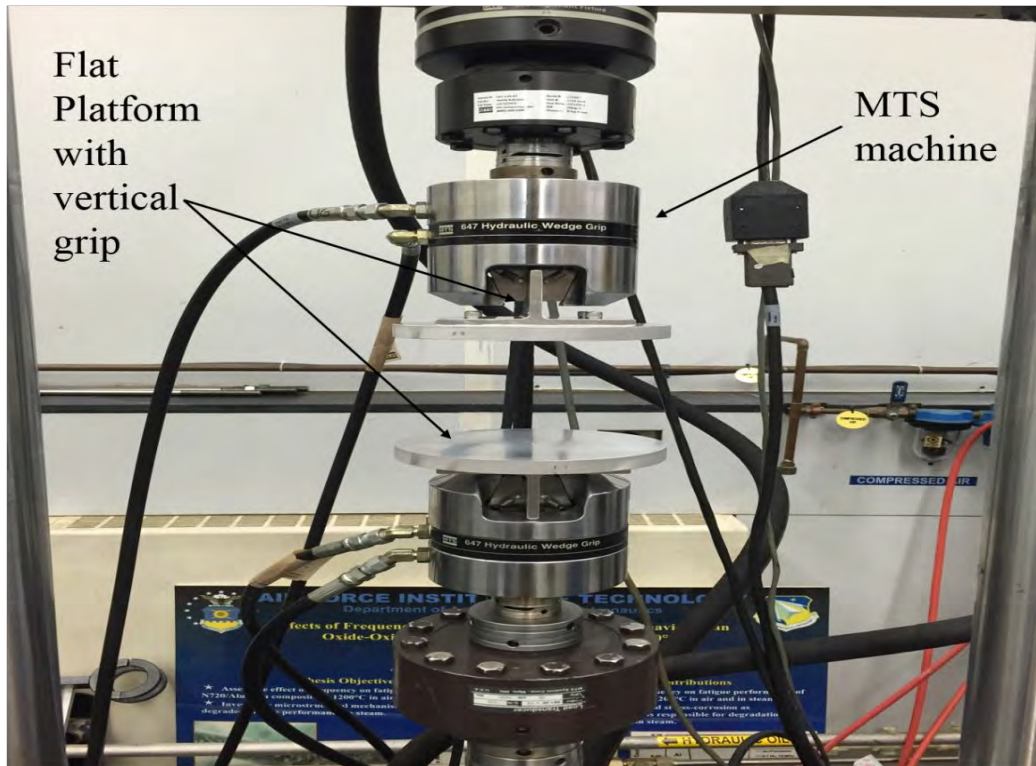
Figure 23: MTS machine with flat platform
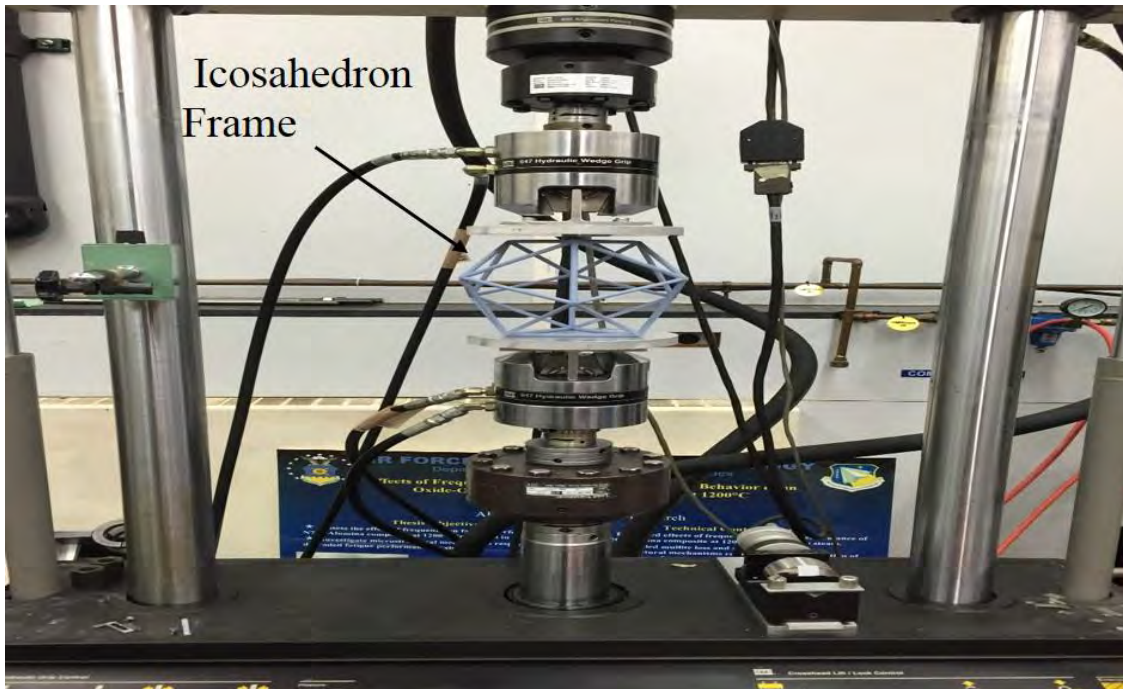
Figure 24: Icosahedron frame with flat platform
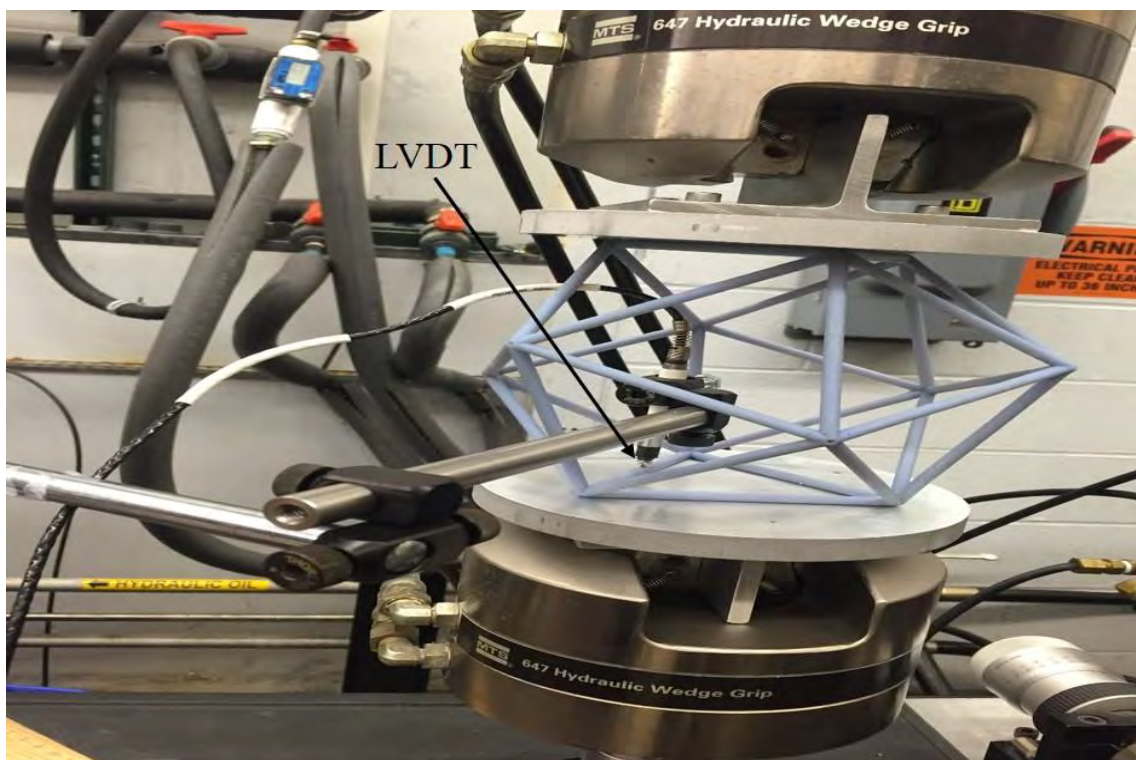
Figure 25: LVDT attached to icosahedron frame

A high-speed camera was used to capture the deformation of the beams, as shown in Figure 26. A BASLER camera (model number acA2000-165um) with a 20-frames per second (fps) was used to record the beam deformation.
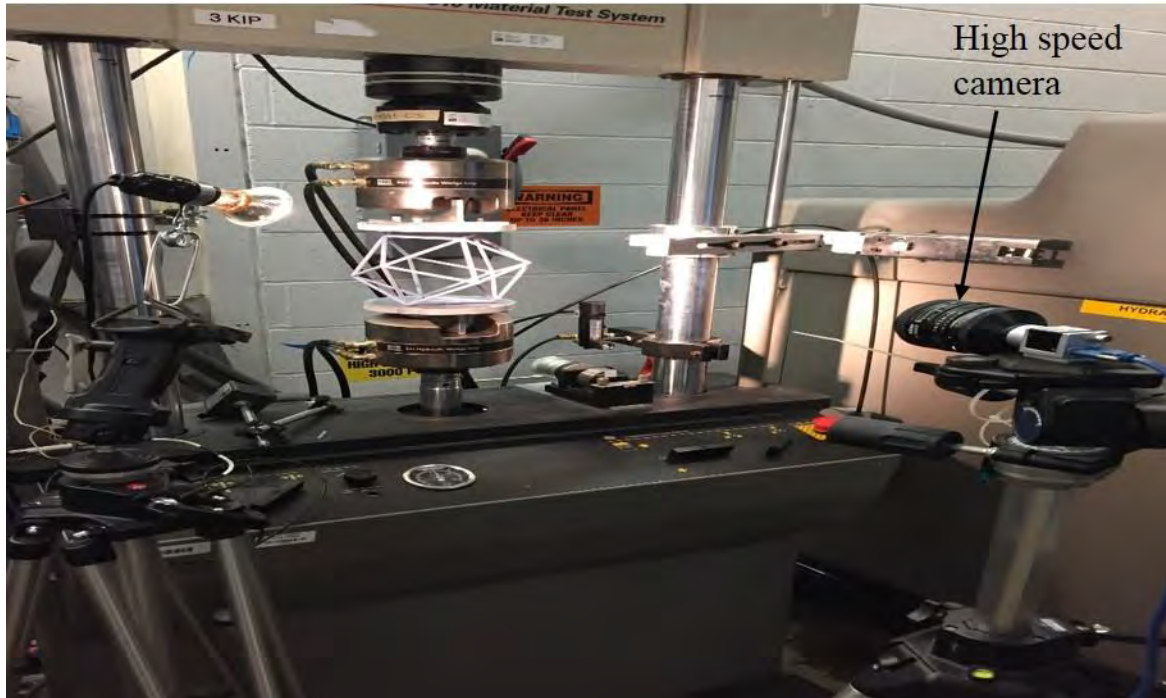
Figure 26: High-speed camera

3.4.1 Mechanical Testing Procedure

The MPT application was opened within the MTS FlexTest 40 Station Manager. The procedure was run in displacement control, at constant rate of 0.02 mm/s (0.047 inches/min). Once the icosahedron was aligned with the fixture, the test was initiated. After the test was completed, the data, which was stored as a .DAT file, was process in Microsoft Excel.

3.5 Summary

The purpose of this chapter is to discuss the design of the frame. The analysis techniques used in this thesis are discussed, and afterwards, the experimental test setup with mechanical testing procedure is presented.

IV. Analysis and Results

4.1 Overview

The modeling techniques for the analysis of an icosahedron structure, and the experimental test setup, were detailed in chapter three and are repeated in this chapter. This chapter will discuss the results of the equal W/B between the seven and the four-inch icosahedrons with a static applied load, and the experimental results with a comparison between the finite elements model and an experiment.

4.2 Comparison with the same W/B

Two icosahedrons were compared with the equal W/B between seven-inch diameter and four-inch diameter, which made the cross section of the beams for the seven-inch greater than the four-inch. The load was applied until the structure reached the collapse mode. In this comparison, a linear bifurcation analysis was conducted to visualize the possible collapse mode's shapes, and a nonlinear buckling analysis was conducted to visualize the buckling. The following sections discuss the linear and nonlinear analysis.

4.2.1 Icosahedron linear buckling analysis

A linear bifurcation analysis is a process that estimates the eigenvalue, which represent the critical (bifurcation) loads and the mode shapes. This procedure is only used to estimate the mode shapes of the icosahedral structure and to visualize the possible collapse mode shapes. The FE model calculates many buckling modes, but only the first mode is relevant, since higher modes have no chance of taking place because the

structure will have already collapsed [27]. The eigenvalues were 650 N for the seven-inch model (Figure 27), and 226 N for the four-inch model (Figure 28). To carry out an eigenvalue-eigenvector analysis within ABAQUS, the perturbation method had to be used. In order to do the analysis, the step was changed to linear perturbation, buckle instead of (static, and general) to carry out the evaluation of eigenvalue-eigenvector analysis.
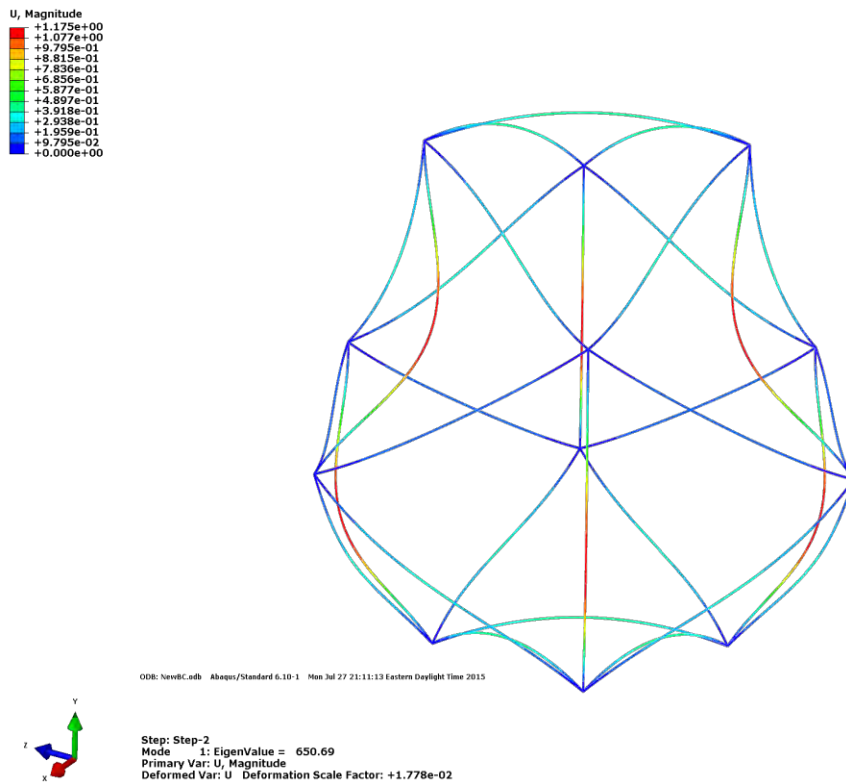
Figure 27: Mode 1 in the seven-inch icosahedron
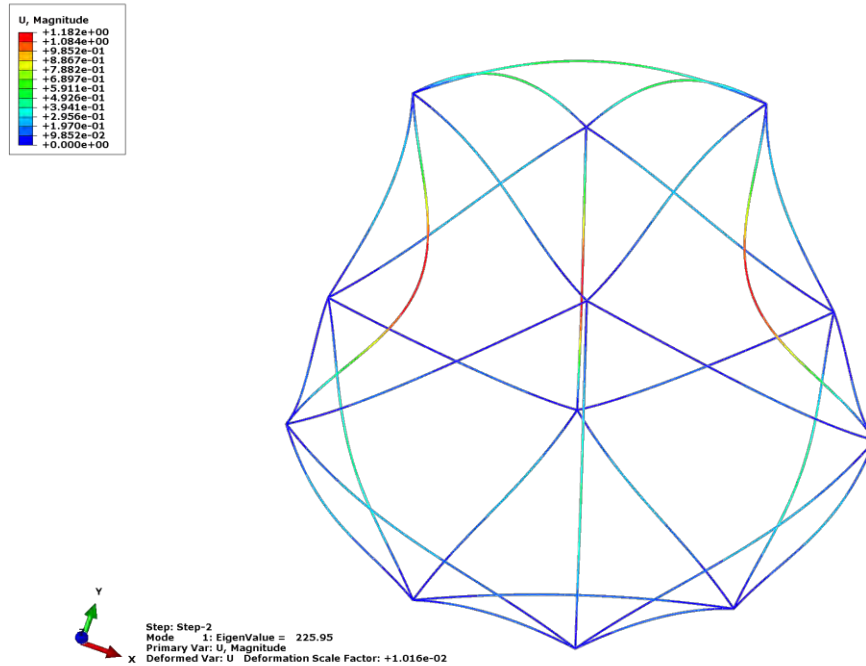
Figure 28: Mode 1 in the four-inch icosahedron

The first eigenvector for both comparisons between the seven-inch and the four-inch eigenvector were very similar. Even though there was a positive difference of 250% in the eigenvalues, the sizes does not make any difference.

4.2.2 Icosahedron nonlinear buckling analysis

A nonlinear buckling analysis was conducted, to compare between equal W/B for the seven and four-inch icosahedron, which used the VeroBlue material. The first set of material properties [13] of VeroBlue were used in comparing two icosahedrons with the same weight to buoyancy Ratio (W/B). The second set of material properties [12] was used in comparing the experimental results with the seven-inch 3D model, which was larger than the original design, as presented in chapter 3.

The load was applied until the structure reached the collapse mode. For the seven-inch, the load was 720 N (Figure 29) and for the four-inch, the load was 255 N (Figure 30). The load was applied at the top of the three vertices. It should be noted that the beam at the loading and support regions show bending. Therefore, the boundary condition removing rotational resistance is correct.
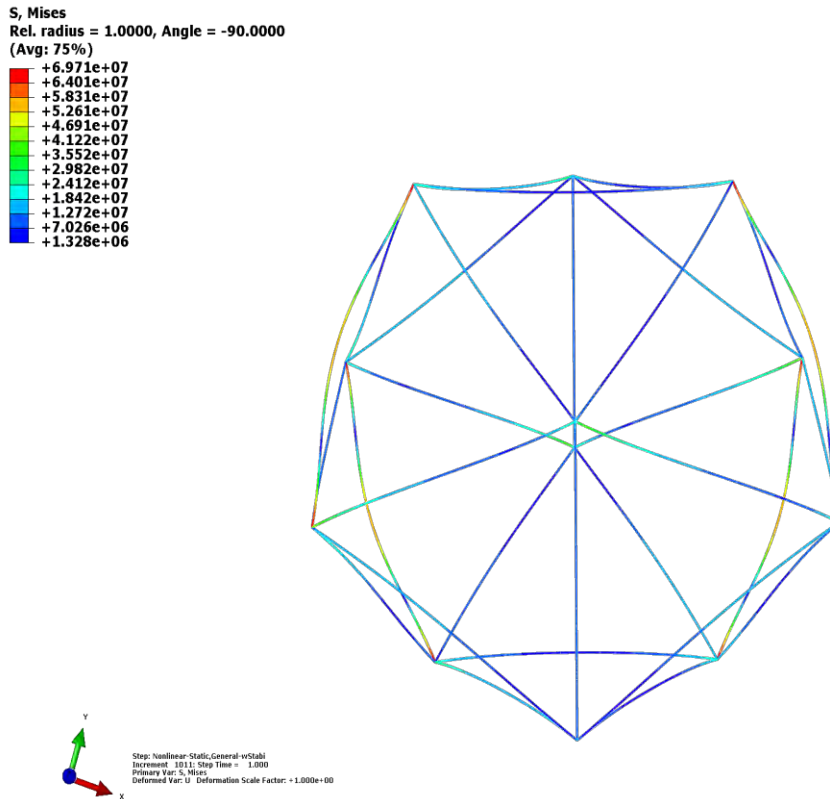
Figure 29: Seven-inch icosahedron
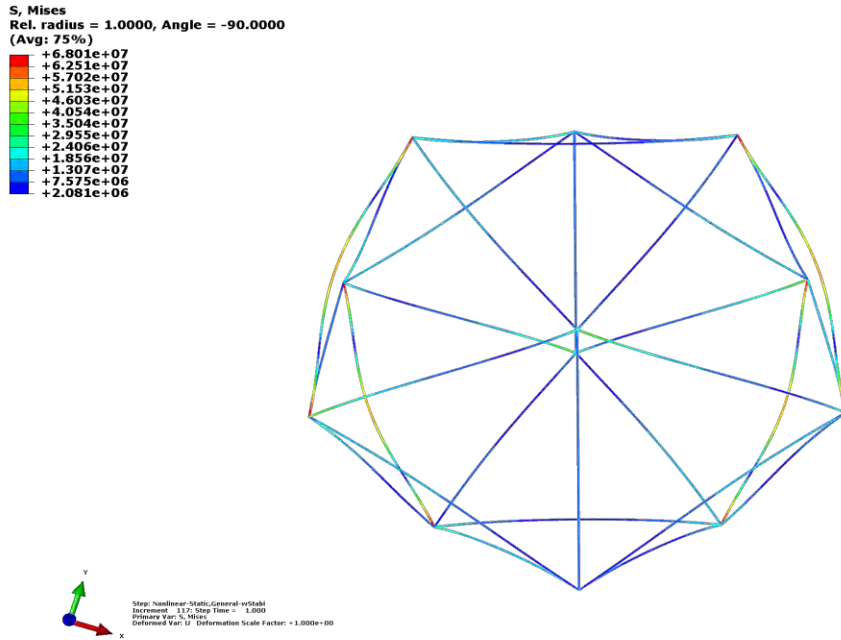
Figure 30: Four-inch icosahedron

In this comparison, the buckle and material failure were considered. The material failed at 63 MPa [13]. Figure 31 and Figure 32 show the stress at material failure, with the reaction force at the same failure stress for the seven-inch model and the four-inch model, respectively. The force was the total of the reaction forces acting at the three vertices. Figure 33 and Figure 34 shows the buckling in the icosahedron for the seven-inch and the four-inch frames, respectively.
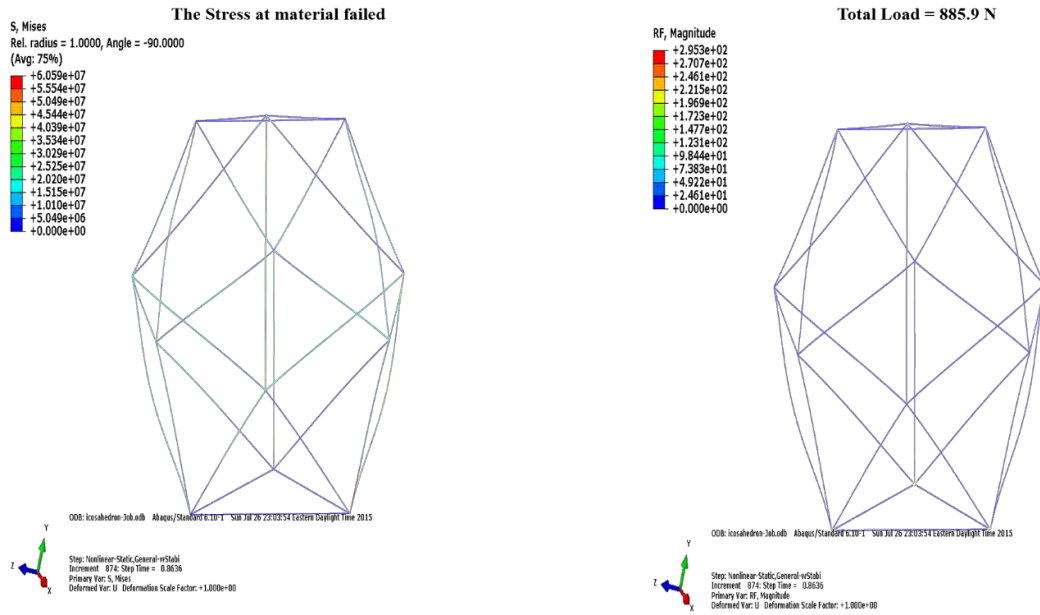
Figure 31: Stress at material failed (left), Reaction force at the same stress (right) for the

seven-inch icosahedron
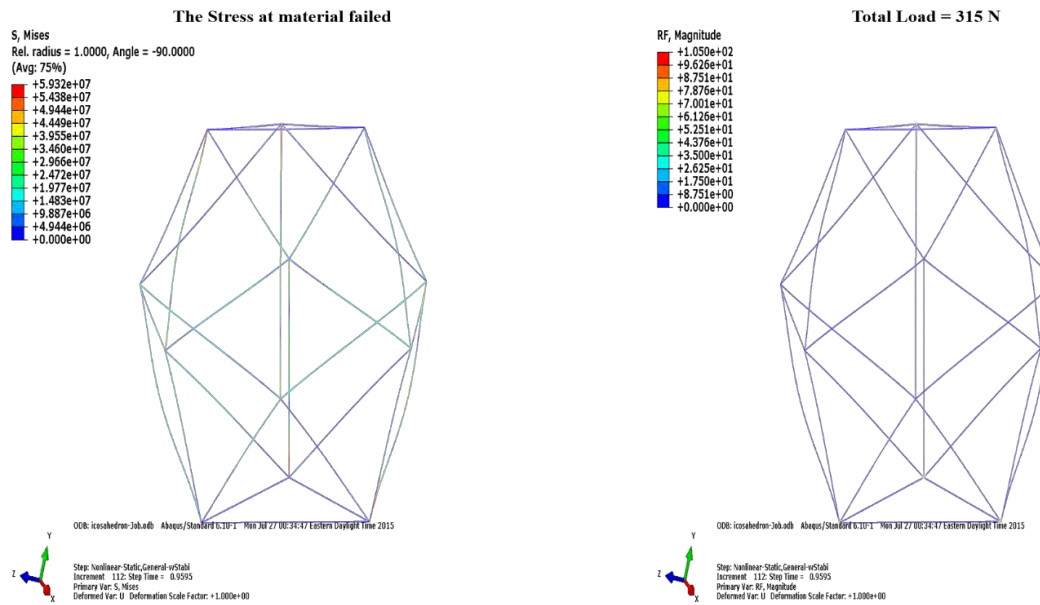
Figure 32: Stress at material failed (left), Reaction force at the same stress (right) for the

four-inch icosahedron

48

The material failed for the seven-inch model at 886 N, and the four-inch model

failed at 315 N, as shown in Figure 31 and Figure 32. The buckling for the icosahedron

was indicated using ABAQUS multiple plot states with deform and undeform shape, as

shown in Figure 33 and Figure 34. The beams started to buckle for the seven-inch and

four-inch at 659 N and 228 N, respectively. Figure 35 and Figure 36 show the plots

between load versus displacement for the seven-inch and the four-inch, respectively.
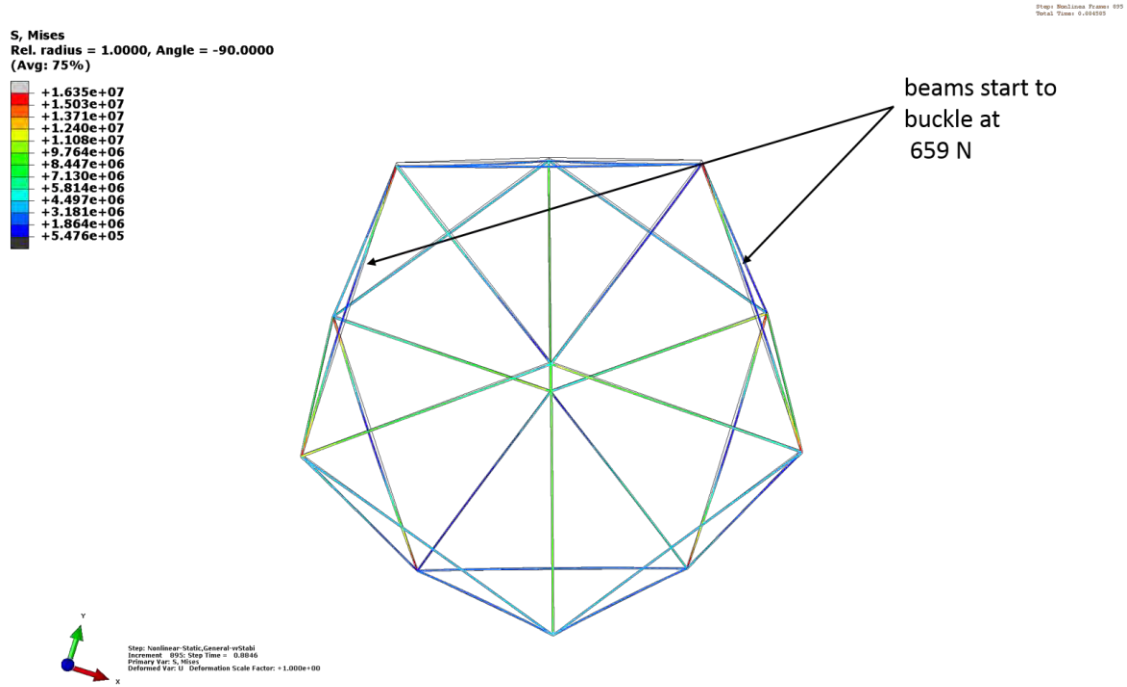
Figure 33: Beams start to buckle for the seven-inch
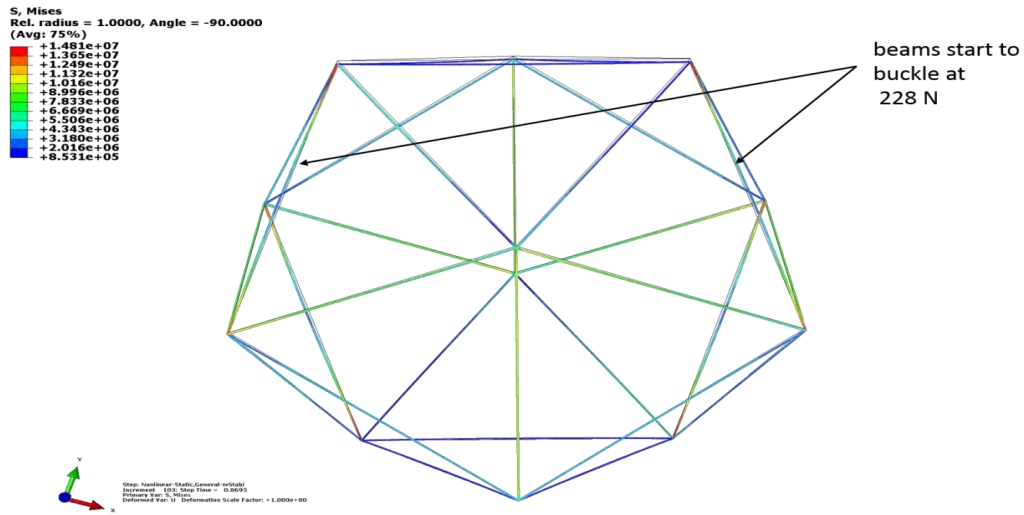
Figure 34: Beams start to buckle for four-inch
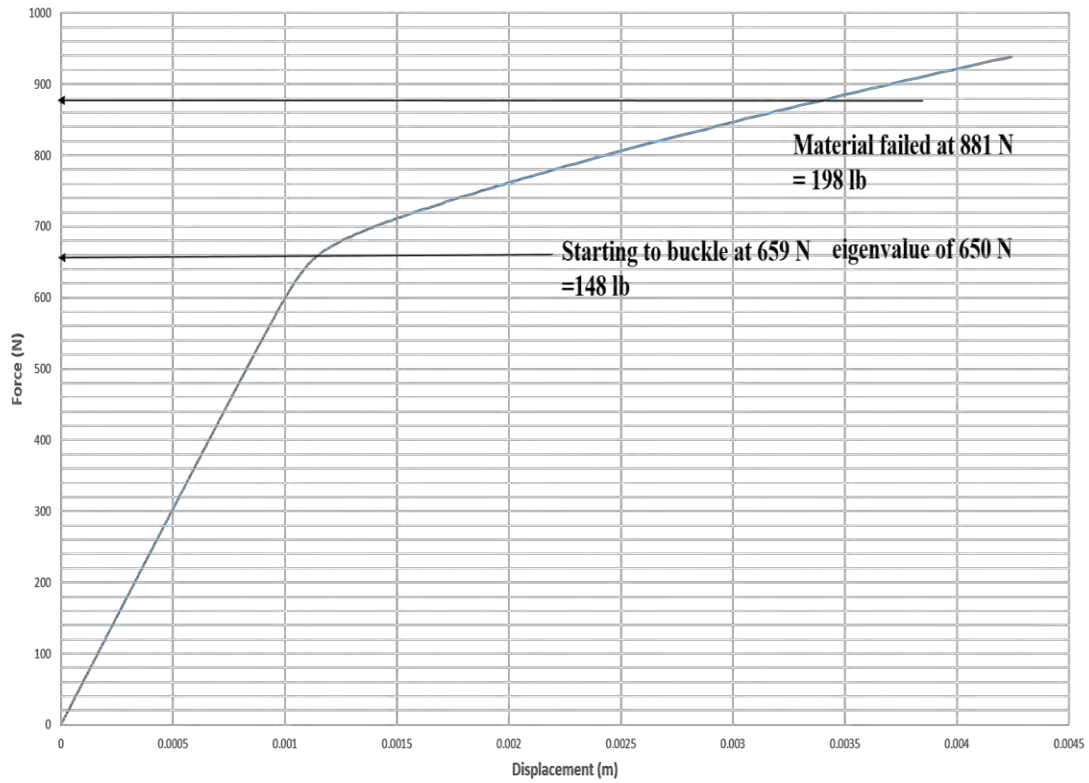
Figure 35: Load vs Displacement for the seven-inch model
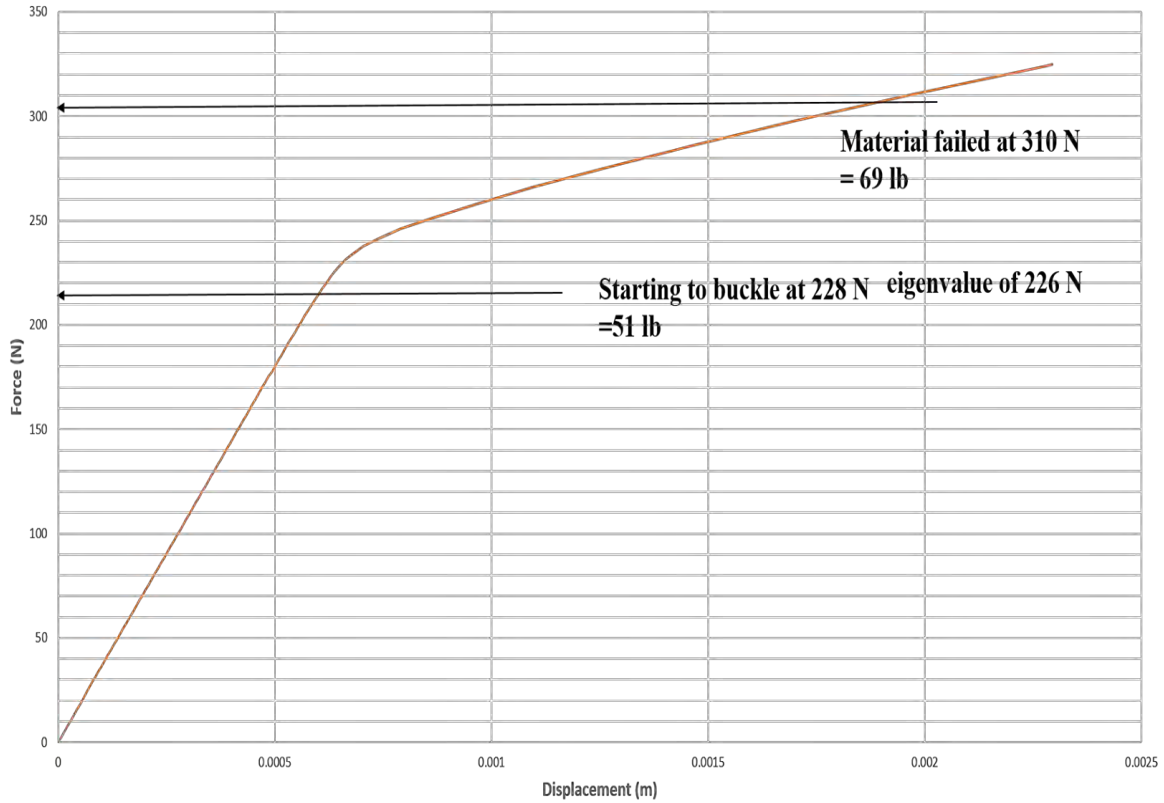
Figure 36: Load vs Displacement for the four-inch model

In Figure 35, the model was linear until it reached 1.2 mm displacement then started to become nonlinear. In Figure 36, the model reached 0.65 mm until it started to become nonlinear. The models in ABAQUS do not consider the material failure criteria, which made the structure stiffer and led to continuously rising load.

For the seven-inch model, beams show nonlinearity at 659 N (148 lb.) which was close to the eigenvalue (650 N), and the material failed at 881 N (198 lb.). The four-inch model a beam start to buckle at 228 (51 lb.), and the eigenvalue was 226 N, and the material failed at 310 N (69 lb.). The study shows that an equivalent (W/B) between frame dimensions is not a beneficial way to expand the design of the icosahedron, since

51

there is virtually no similarity in stress between the different frames. It was shown by Cranston [5] that it is possible for an entire icosahedron with an attached membrane to have an equal stress distribution, and thus possible to design for one (W/B) ratio at any elevation.

4.3 Comparison FE model with experimental

Using Boston University material properties [13], the results here were more than 40% different compared to the experimental results as shown in Figure 37. The difference in the results led to investigate the cause. The first step was measuring the actual size of 3D model, which was actually 7.2 inch in diameter. The second step was to measure each beam diameter, which varied due to the manufacturing uncertainty. The last step was to research the material properties, which was the second study as detailed in chapter 2.

In this comparison, the material properties for the FE model were varied, detailed in chapter 2, Table 2 [12]. The experimental test setup was detailed in chapter 3, as shown in Figure 40 and Figure 41. Three different elastic modulus (E) were chosen in this research: the lowest value which was 1.176 GPa, the largest value which was 1.874 GPa and the mid-value which was 1.577 GPa. Eigenvalue analysis was carried out to estimate the buckling of the beams as shown in Figures 38 to 40. Then, the displacement control was applied to the FE model. For the experiment test, only the load data was considered. A high-speed camera, Figure 42, was used it to capture the buckling and compare to the FE model as shown in Figures 43 to 45.
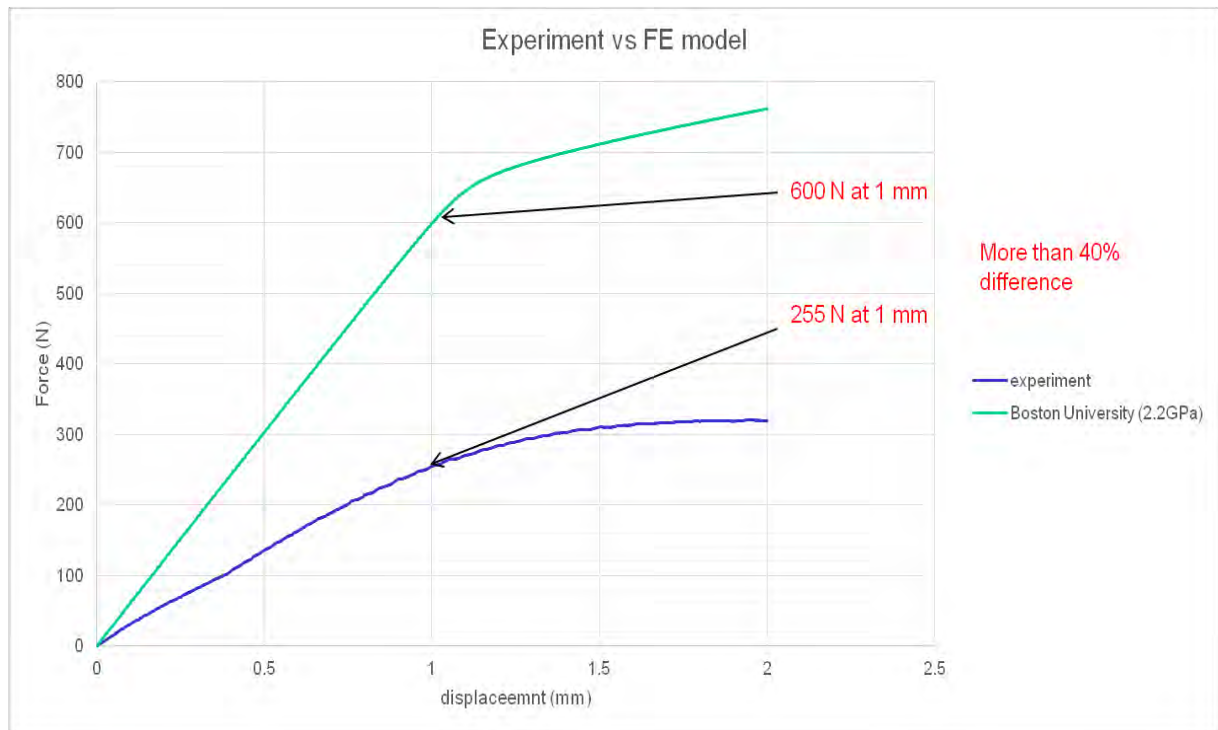
Figure 37: Experiment result vs BU material properties

Eigenvalue for 1.874 GPa = 481.98
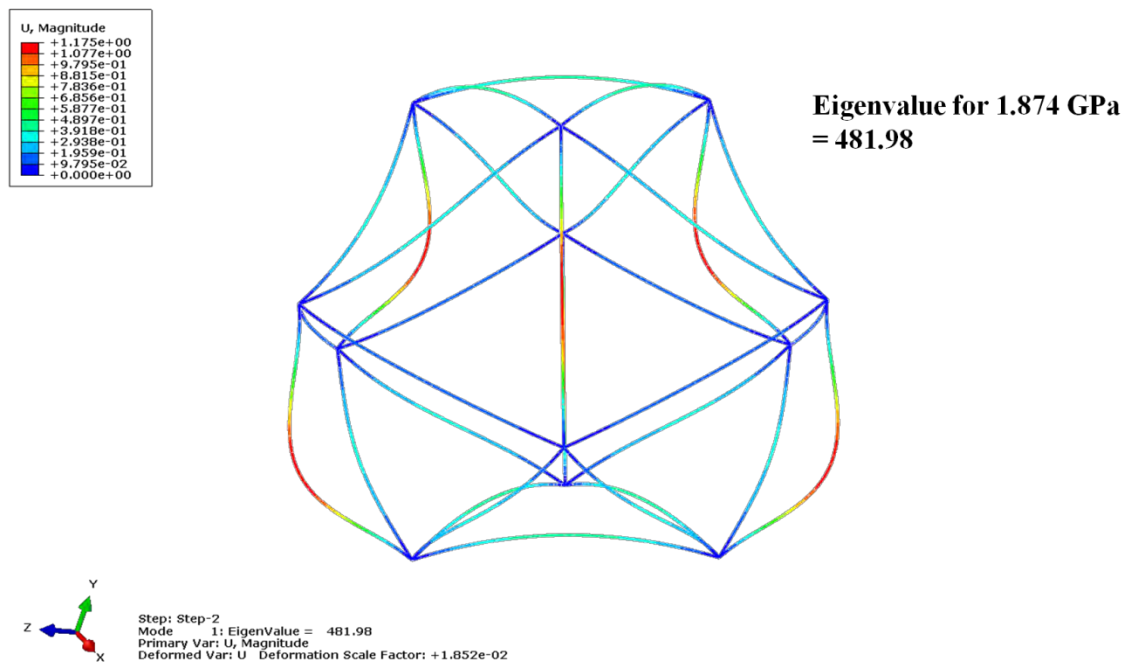
Figure 38: Eigenvalue for 1.874 GPa
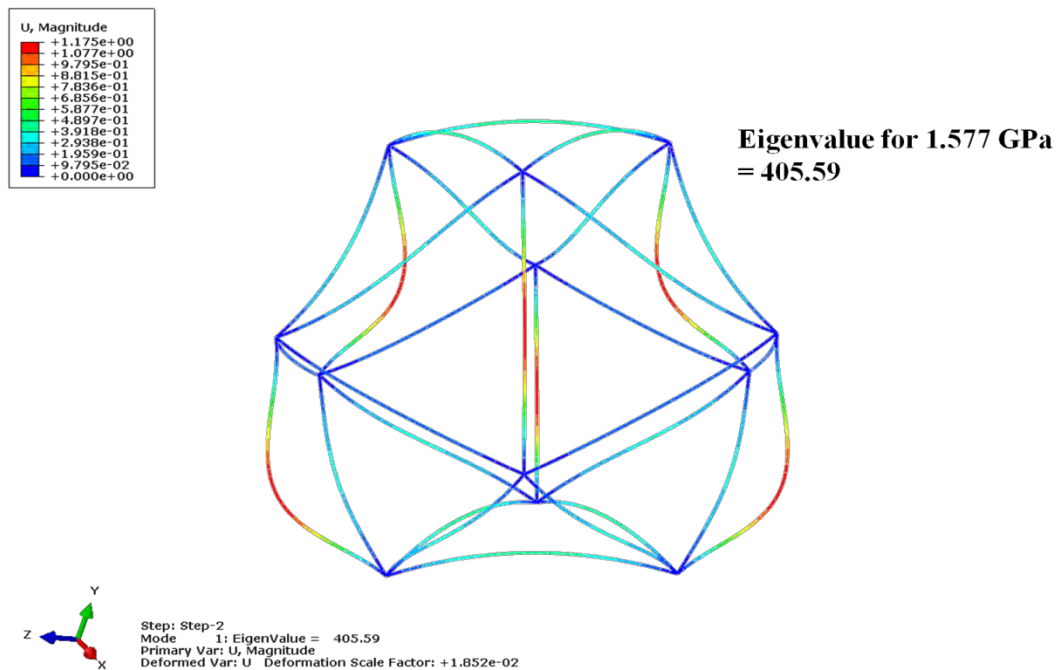
Figure 39: Eigenvalue for 1.577 GPa
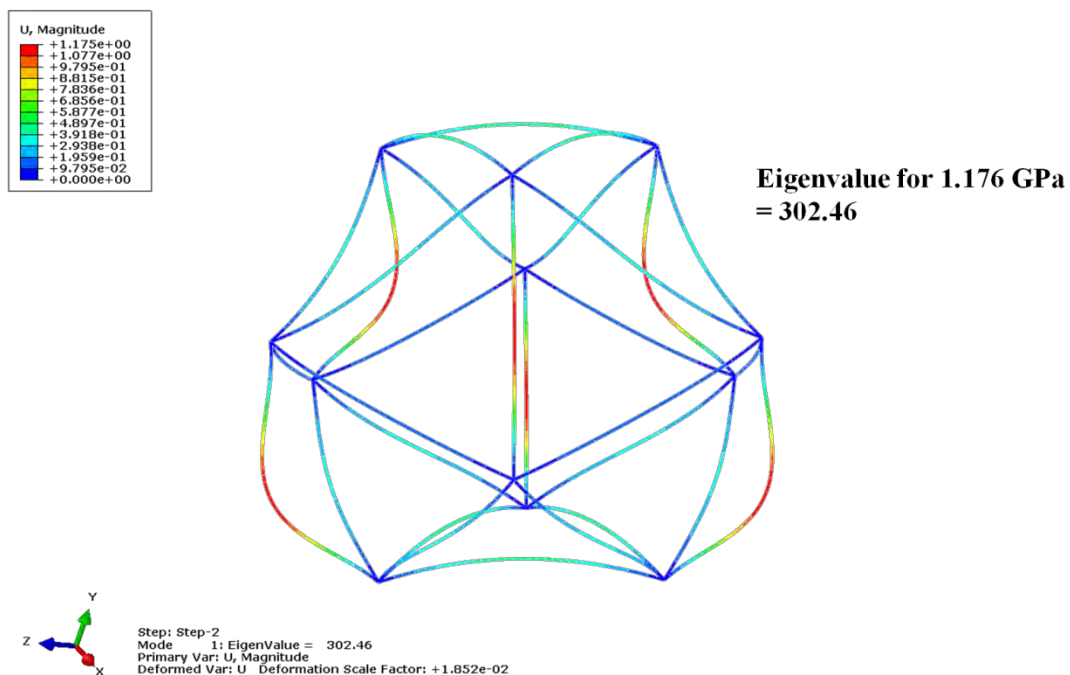
Figure 40: Eigenvalue for 1.176 GPa
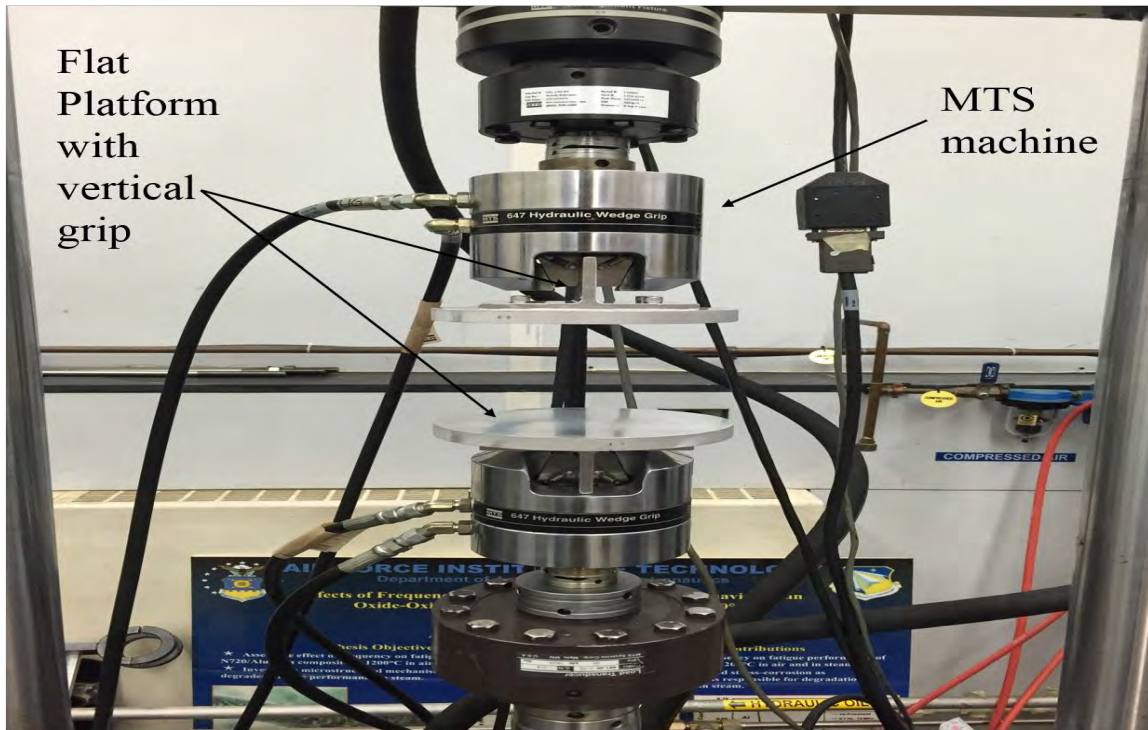
Figure 41: Icosahedron Frame with flat platform
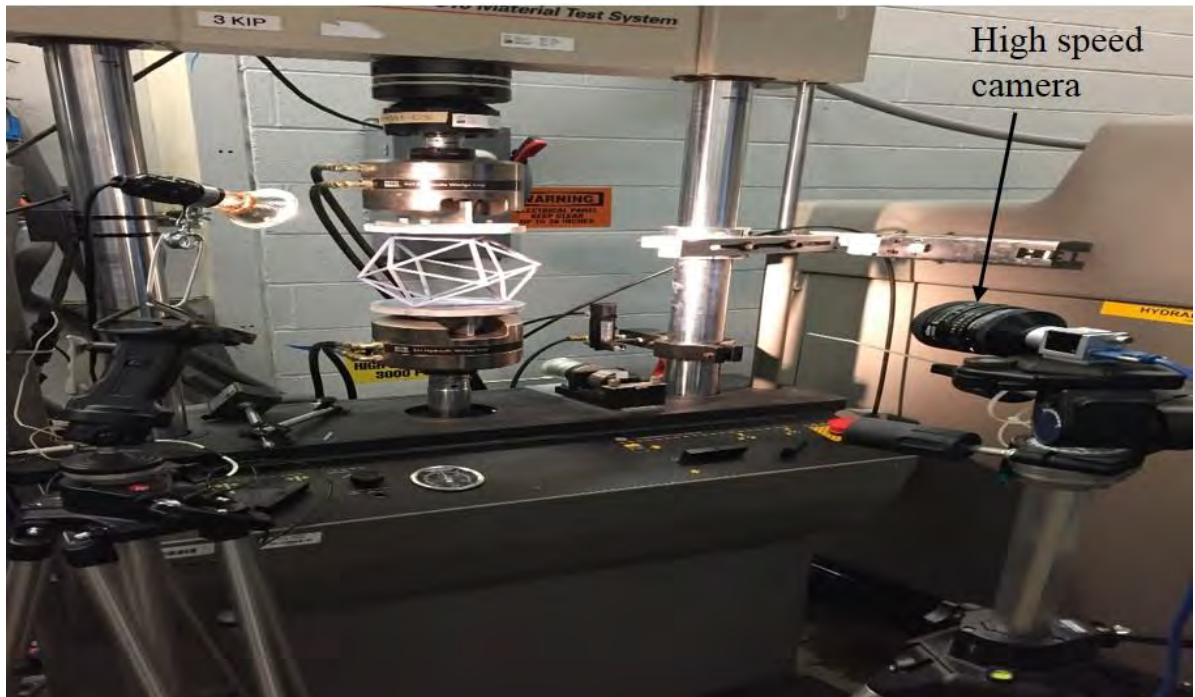
Figure 42: High-speed camera
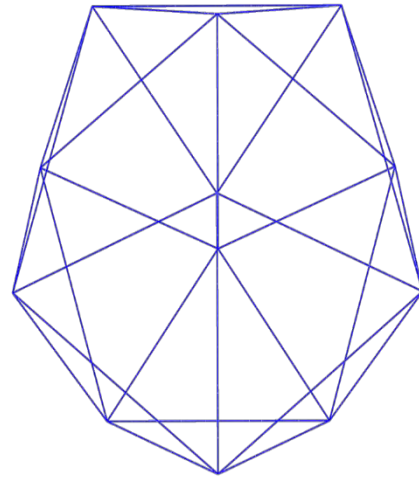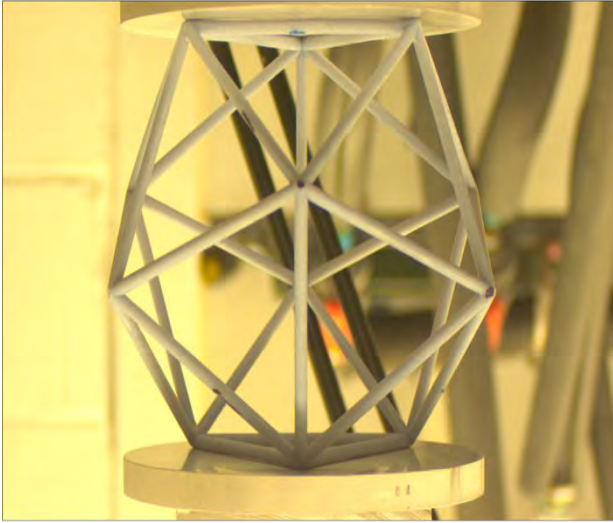
Figure 43: Icosahedron before applied the load
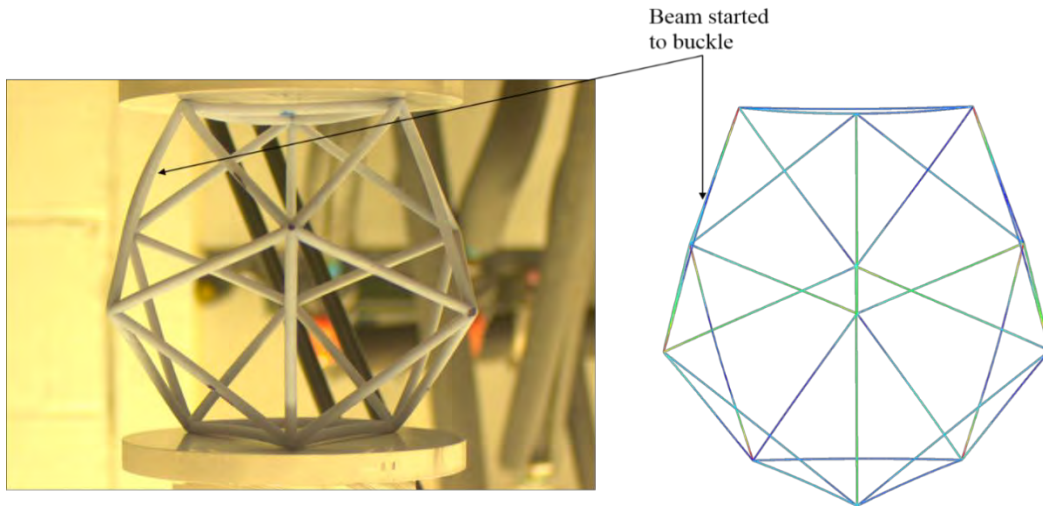
Figure 44: Displacement control at 2 mm
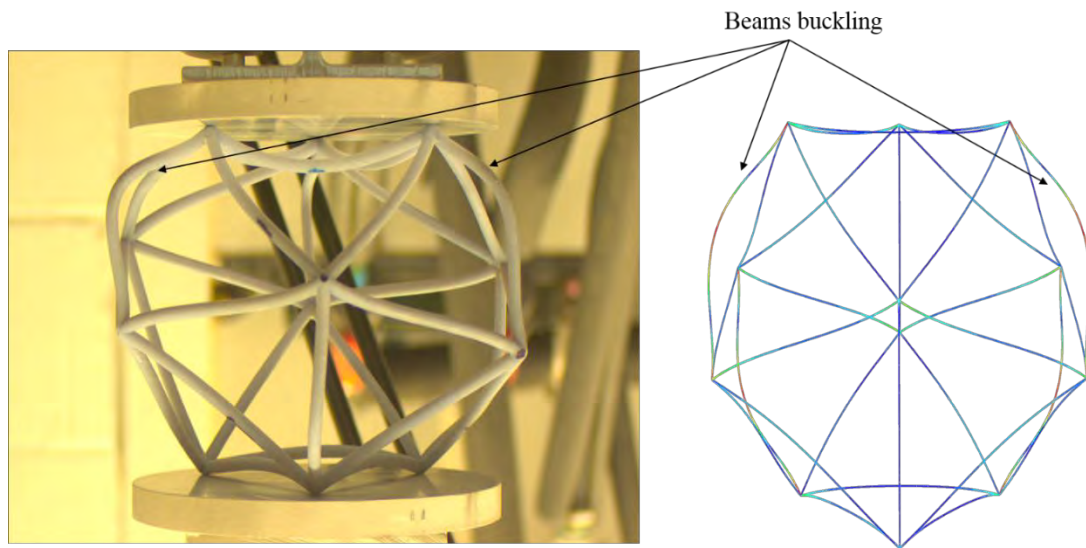
Figure 45: Displacement control at 14 mm

Figure 46 shows the comparison between the FE model with different material properties and the experimental results. The eigenvalues for the three different elastic modulus (E) 1.874 GPa, 1.577 GPa and 1.176 GPa, were 481.98 N, 405.59 N and 302.46 N, respectively. These values are the start of nonlinear behavior for each case considered.
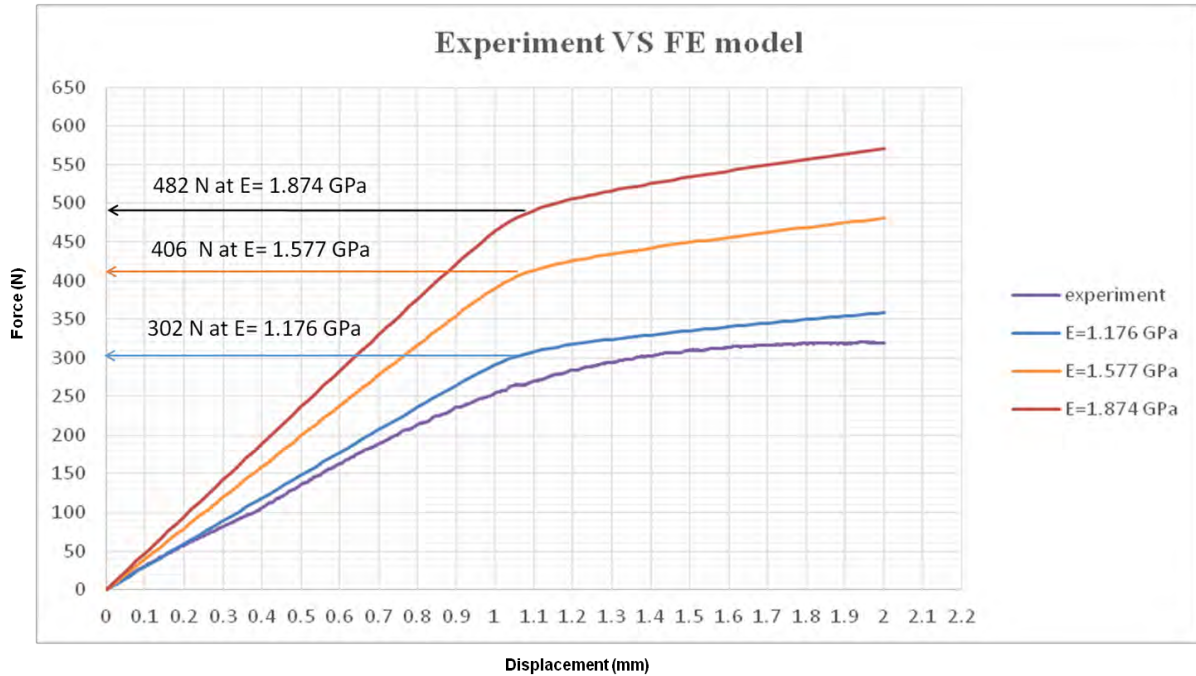
Figure 46: Comparison between FE model and experimental

The lowest modulus is close to the experiment results, which means the material properties of the 3D model is much lower than what Objet the manufacturer, reported [17]. Comment related to determination of this low value of E was made in chapter 2.

4.4 Summary

The compressive load with the same weight to buoyancy ratio for the seven-inch diameter and the four-inch diameter as an equality function causes the frame to get stiffer as the dimension get larger. In addition, for an equal (W/B) the internal stress per frame was variable. For the experimental results, the lowest elastic modulus used in the FE model matched the experiment (The author carried out a nano indentation test [14] and obtained an E Value of 1 GPa, therefore it appears the lowest E value is appropriate in the experiment).

58

V. Conclusions and Recommendations

5.1 Overview

The previous chapters in this research have discussed the history of LTAVs, the nonlinear analysis of the icosahedron frame, and the methodology; developing the techniques necessary for the icosahedron design; comparison between two equal weights to buoyancy ratios, a seven-inch and a four-inch icosahedron; as well as comparisons between the seven-inch icosahedron with the experiment conducted. This chapter will report the important developments that transpired during the research, with recommendations for future research.

5.2 Conclusion of Research

- The same W/B ratio made the cross section of the beams for the seven-inch greater than the four-inch, which led to non-similar distribution of stress.

- Applying a compressive load to the top of the icosahedron structure produced local beam bending near the loading, which removed certain rotational restraints for the boundary condition applied.

- Results showed that the onset of nonlinearity was very close to the first eigenvalue of the frame.

- Experiments on the VeroBlue material need to be carried out for all analyses.

- The dimension for the seven-inch was changed in the 3D printer, and therefore extensive fine-tuning on the measurements, not only for the geometry, but for the material properties, was necessary.

59

- The lowest modulus is close to the experiment results, which means the material properties of the 3D model is much lower from what the Objet manufacturer reported.

- The results from the experiments prove that the method of analysis for the frame is correct.

5.3 Significance of Research

The nonlinear static response to an icosahedron frame has been evaluated, and the computer FEA model used in researching the structure has been verified. An experimental test setup was developed, and a comparison to the FEA model was made to verify the results. The nonlinear behavior exhibited by the icosahedron frame was characterized for certain loads and boundary conditions. This development will help to verify the FEA model with the experimental test.

5.4 Recommendations for Future Research

- The comparison between two equally weight to buoyancy ratio icosahedrons were used only for the frame. Adding the membrane to the frame on the icosahedron will result in a more accurate response prediction.

- The experimental analysis was conducted using only the frame. Using a skin material such as Kapton tape to replicate the membrane, will envelope future vacuum icosahedron LTAV.

- A complete evaluation of the material properties produced in any 3D additive

  manufacturing process must be carried out if analysis and experiments are to be

  properly compared. Published material properties values may not apply to a

  specific situation.

Appendix A: MATLAB Codes

The MATLAB codes are used to generate the Python code for icosahedron model in ABAQUS. These codes were generated by Adorno-Rodriguez [18]. The codes are to setup the geometry of the coordinate icosahedron frame and the membrane in that frame and the material related to that frame. The only change made by the author was in (Main.m) file to setup the geometry of the vertices for the frame. This required modifying the radius of the icosahedron (highlight in red, see page 64) everything else such as, the geometry of the beams, the load apply on the frame and the material properties were represented in ABAQUS.

A.1 Seven-inch icosahedron model (Main.m)

```matlab
clc; clear all ; close all
% Input
 I.scratch_folder = 'Temp Scratch Files' ;
I.job.num_cores = 1;
I.job.memory_usage = 1024;
I.job.num_GPUs = 0;
% Static Step Info
 I.step.buckle = 0;
I.step.stabilization = 1;
I.step.step_type = 0;
I.step.nonlinear_effects = 'ON' ;
I.step.increment_method = 'AUTOMATIC' ;
I.step.maxnuminc = 100000000;
% Static Riks
 I.step.initial_ArcInc = 0.1;
I.step.min_ArcInc = 1e-12;
I.step.max_ArcInc = 1;
I.step.max_LPF = 2;
% Static General
 I.step.initial_inc = 1e+00;
I.step.max_inc = 1;
I.step.min_inc = 1e-36;
I.step.stabilization_ratio = 0.05;
I.step.stabilization_magn = 0.0002;
% Linear Buckle
 I.step.buck_num_Eigen = 5;
I.step.buck_max_Iter = 30;
I.step.buck_num_vectors = 30;
% Load
 I.load.disp_control = 0;
```

```
I.load.d = -3e2 ;
I.load.P = 101325;
% Skin Sections
 I.section.no_stiffness_skin = 0;
I.section.membrane = 1;
% Shell Only
 I.section.skin_section_idealization = 'NO_IDEALIZATION' ;
I.section.skin_section_location = 'MIDDLE_SURFACE' ;
% Tie Constraint
 I.tie.rotations = 'OFF' ;
% Mesh
 I.mesh.skin_element_type1 = 'M3D3' ;
I.mesh.skin_element_type2 = 'M3D3' ;
I.mesh.skin_element_shape = 'TRI' ;
I.mesh.skin_seed_number = 18 ;
2
 I.mesh.frame_element_type = 'B32' ;
I.mesh.frame_seed_number = 18 ;
I.mesh.rays_element_type = 'B32' ;
I.mesh.rays_seed_number = 18 ;
I.mesh.stiff_element_type = 'B32' ;
I.mesh.stiff_seed_number = 18 ;
% Parameters for W/B ratio calculation
 I.W_B.rho = 1.2754;
I.W_B.g = 9.81;
I.W_B.skin = 0.4;
I.W_B.frame = 0.5;
I.W_B.rays = 0;
I.W_B.stiff = 0;
I.W_B.To = 293.15;
I.W_B.Ti = I.W_B.To;
I.W_B.Po = 101325;
% Geometry and Material Selection
% Material Selection
% rho nu E Sy ;
 mat1 = [1870 0.3 440e9 3.73e9 ];
mat2 = [1560 0.37 303e9 5.8e9 ];
mat3 = [2700 0.12 757e9 75.7e9 ];
mat4 = [2570 0.33 400e9 3.6e9 ];
mat5 = [1650 0.2 1000e9 10e9 ];
mat6 = [1844 0.18 303e9 0.4e9 ];
mat7 = [2650 0.18 379e9 1.7e9 ];
mat8 = [2800 0.33 738e9 0.14e9 ];
mat9 = [247 0.33 5.76e9 0.024e9];
mat10= [970 0.33 172e9 3.0e9 ];
% Material Assignment
 matf = mat5;
mats = mat5;
matr = mat5;
matst= mat5;
I.materials.frame_density = matf(1); I.materials.frame_poisson = matf(2);
I.materials.frame_modulus = matf(3); I.materials.frame_yield = matf(4);
I.materials.skin_density = mats(1); I.materials.skin_poisson = mats(2);
I.materials.skin_modulus = mats(3); I.materials.skin_yield = mats(4);
```

```matlab
I.materials.rays_density = matr(1); I.materials.rays_poisson = matr(2);
I.materials.rays_modulus = matr(3); I.materials.rays_yield = matr(4);
I.materials.stiff_density = matst(1); I.materials.stiff_poisson = matst(2);
I.materials.stiff_modulus = matst(3); I.materials.stiff_yield = matst(4);
% Geometry (icosahedron)
 I.geometry.r = 0.1778/2; % icosahedron radius, m;% This is the only changes in the code
 I.geometry.rays = 0;
I.geometry.stiff = 0;
I.section.hollow_profile_rays = 1;
I.section.hollow_profile_stiff= 1;
I.section.hollow_profile = 1;
3
 c1 = 0.05;
c2 = 0.05;
c3 = 0.05;
for  i = 1
I.geometry.skin_thickness = I.geometry.r*I.W_B.rho*I.W_B.skin/...
 (3.77523*I.materials.skin_density);
if  I.section.hollow_profile == 1
I.geometry.frame_beam_radius = I.geometry.r*sqrt(I.W_B.frame*I.W_B.rho/...
 (39.0742*(2*c1-c1^2)*I.materials.frame_density));
I.geometry.frame_beam_thickness = c1*I.geometry.frame_beam_radius;
else
 I.geometry.frame_beam_radius = sqrt(I.geometry.r^2*I.W_B.rho*I.W_B.frame/...
 (39.0742*I.materials.frame_density));
I.geometry.frame_beam_thickness = I.geometry.frame_beam_radius;
end
if  I.section.hollow_profile_rays == 1
I.geometry.rays_beam_radius = I.geometry.r*sqrt(I.W_B.rays*I.W_B.rho/...
 (19.82*(2*c2-c2^2)*I.materials.rays_density));
I.geometry.rays_beam_thickness = c2*I.geometry.rays_beam_radius;
else
 I.geometry.rays_beam_radius = sqrt(I.geometry.r^2*I.W_B.rho*I.W_B.rays/...
 (19.82*I.materials.rays_density));
I.geometry.rays_beam_thickness = I.geometry.rays_beam_radius;
end
if  I.section.hollow_profile_stiff == 1
I.geometry.stiff_beam_radius= I.geometry.r*sqrt(I.W_B.stiff*I.W_B.rho/...
 (45.34*(2*c3-c3^2)*I.materials.stiff_density));
I.geometry.stiff_beam_thickness = c3*I.geometry.stiff_beam_radius;
else
 I.geometry.stiff_beam_radius= sqrt(I.geometry.r^2*I.W_B.rho*I.W_B.stiff/...
 (45.34*I.materials.stiff_density));
I.geometry.stiff_beam_thickness = I.geometry.stiff_beam_radius;
end
end
% FEA Analysis
 I.step.buckle = 0;
O1 = icosahedron_fea_inner2(I);
```

Adorno-Rodriguez [18] generated Python codes to use in ABAQUS. The only modification was in Python file (frame.py). B.1 below shows the deleted portion of the code, which was replaced by the Python file (Var_icosahedron.py) as shown in B.2 that was generated by the MATLAB code (Appendix A) to generate the geometry of the vertices for the frame. Similar modification was used to analyze the other models.

B.1 frame.py

```
# Sets Working Directory
**********************************************************************
os.chdir(path)

# Load variables
**********************************************************************
execfile('Var_frame.py')
```

B.2 Var_icosahedron.py

```
p_array = [(0.000000,0.000000,0.088900),(0.079515,0.000000,0.039757),(0.024571,0.075623,0.039757),(-
0.064329,0.046737,0.039757),(-0.064329,-0.046737,0.039757),(0.024571,-
0.075623,0.039757),(0.064329,0.046737,-0.039757),(-0.024571,0.075623,-0.039757),(-
0.079515,0.000000,-0.039757),(-0.024571,-0.075623,-0.039757),(0.064329,-0.046737,-
0.039757),(0.000000,0.000000,-0.088900),]

k =
[(1,2,3),(1,3,4),(1,4,5),(1,5,6),(1,6,2),(12,7,8),(12,8,9),(12,9,10),(12,10,11),(12,11,7),(7,2,3),(3,7,8),(8,3,4),(
4,8,9),(9,4,5),(5,9,10),(10,5,6),(6,10,11),(11,2,6),(2,7,11),]

fc = [(0.034695,0.025208,0.056138),(-0.013252,0.040787,0.056138),(-0.042886,0.000000,0.056138),(-
0.013252,-0.040787,0.056138),(0.034695,-0.025208,0.056138),(0.013252,0.040787,-0.056138),(-
0.034695,0.025208,-0.056138),(-0.034695,-0.025208,-0.056138),(0.013252,-0.040787,-
0.056138),(0.042886,-0.000000,-0.056138),(0.056138,0.040787,0.013252),(0.021443,0.065994,-
0.013252),(-0.021443,0.065994,0.013252),(-0.056138,0.040787,-0.013252),(-
0.069391,0.000000,0.013252),(-0.056138,-0.040787,-0.013252),(-0.021443,-
0.065994,0.013252),(0.021443,-0.065994,-0.013252),(0.056138,-0.040787,0.013252),(0.069391,-
0.000000,-0.013252),]

np = [(0.017348,0.012604,0.072519),(0.057105,0.012604,0.047948),(0.029633,0.050415,0.047948),(-
0.006626,0.020393,0.072519),(0.005659,0.058205,0.047948),(-0.038791,0.043762,0.047948),(-
```

0.021443,0.000000,0.072519),(-0.053607,0.023369,0.047948),(-0.053607,-0.023369,0.047948),(-0.006626,-0.020393,0.072519),(-0.038791,-0.043762,0.047948),(0.005659,-0.058205,0.047948),(0.017348,-0.012604,0.072519),(0.029633,-0.050415,0.047948),(0.057105,-0.012604,0.047948),(0.006626,0.020393,-0.072519),(0.038791,0.043762,-0.047948),(-0.005659,0.058205,-0.047948),(-0.017348,0.012604,-0.072519),(-0.029633,0.050415,-0.047948),(-0.057105,0.012604,-0.047948),(-0.017348,-0.012604,-0.072519),(-0.057105,-0.012604,-0.047948),(-0.029633,-0.050415,-0.047948),(0.006626,-0.020393,-0.072519),(-0.005659,-0.058205,-0.047948),(0.038791,-0.043762,-0.047948),(0.021443,-0.000000,-0.072519),(0.053607,-0.023369,-0.047948),(0.053607,0.023369,-0.047948),(0.060233,0.043762,-0.013252),(0.067826,0.020393,0.026505),(0.040355,0.058205,0.026505),(0.023007,0.070809,0.013252),(0.042886,0.056366,-0.026505),(-0.001564,0.070809,-0.026505),(-0.023007,0.070809,-0.013252),(0.001564,0.070809,0.026505),(-0.042886,0.056366,0.026505),(-0.060233,0.043762,0.013252),(-0.040355,0.058205,-0.026505),(-0.067826,0.020393,-0.026505),(-0.074453,0.000000,-0.013252),(-0.066860,0.023369,0.026505),(-0.066860,-0.023369,0.026505),(-0.060233,-0.043762,0.013252),(-0.067826,-0.020393,-0.026505),(-0.040355,-0.058205,-0.026505),(-0.023007,-0.070809,-0.013252),(-0.042886,-0.056366,0.026505),(0.001564,-0.070809,0.026505),(0.023007,-0.070809,0.013252),(-0.001564,-0.070809,-0.026505),(0.042886,-0.056366,-0.026505),(0.060233,-0.043762,-0.013252),(0.067826,-0.020393,0.026505),(0.040355,-0.058205,0.026505),(0.074453,-0.000000,0.013252),(0.066860,0.023369,-0.026505),(0.066860,-0.023369,-0.026505),]

p1=(0.000000,0.000000,0.088900)
p2=(0.079515,0.000000,0.039757)
p3=(0.024571,0.075623,0.039757)
p4=(-0.064329,0.046737,0.039757)
p5=(-0.064329,-0.046737,0.039757)
p6=(0.024571,-0.075623,0.039757)
p7=(0.064329,0.046737,-0.039757)
p8=(-0.024571,0.075623,-0.039757)
p9=(-0.079515,0.000000,-0.039757)
p10=(-0.024571,-0.075623,-0.039757)
p11=(0.064329,-0.046737,-0.039757)
p12=(0.000000,0.000000,-0.088900)

mp12=(0.039757,0.000000,0.064329)
mp13=(0.012286,0.037811,0.064329)
mp23=(0.052043,0.037811,0.039757)
mp13=(0.012286,0.037811,0.064329)
mp14=(-0.032164,0.023369,0.064329)
mp34=(-0.019879,0.061180,0.039757)
mp14=(-0.032164,0.023369,0.064329)
mp15=(-0.032164,-0.023369,0.064329)
mp45=(-0.064329,0.000000,0.039757)
mp15=(-0.032164,-0.023369,0.064329)
mp16=(0.012286,-0.037811,0.064329)
mp56=(-0.019879,-0.061180,0.039757)
mp16=(0.012286,-0.037811,0.064329)
mp12=(0.039757,0.000000,0.064329)
mp62=(0.052043,-0.037811,0.039757)
mp127=(0.032164,0.023369,-0.064329)
mp128=(-0.012286,0.037811,-0.064329)
mp78=(0.019879,0.061180,-0.039757)
mp128=(-0.012286,0.037811,-0.064329)
mp129=(-0.039757,0.000000,-0.064329)

mp89=(-0.052043,0.037811,-0.039757)
mp129=(-0.039757,0.000000,-0.064329)
mp1210=(-0.012286,-0.037811,-0.064329)
mp910=(-0.052043,-0.037811,-0.039757)
mp1211=(0.032164,-0.023369,-0.064329)
mp1210=(-0.012286,-0.037811,-0.064329)
mp1110=(0.019879,-0.061180,-0.039757)
mp127=(0.032164,0.023369,-0.064329)
mp1211=(0.032164,-0.023369,-0.064329)
mp711=(0.064329,-0.000000,-0.039757)
mp211=(0.071922,-0.023369,0.000000)
mp27=(0.071922,0.023369,0.000000)
mp711=(0.064329,-0.000000,-0.039757)
mp112=(0.071922,-0.023369,0.000000)
mp116=(0.044450,-0.061180,0.000000)
mp26=(0.052043,-0.037811,0.039757)
mp610=(-0.000000,-0.075623,0.000000)
mp611=(0.044450,-0.061180,0.000000)
mp1011=(0.019879,-0.061180,-0.039757)
mp105=(-0.044450,-0.061180,0.000000)
mp106=(-0.000000,-0.075623,0.000000)
mp56=(-0.019879,-0.061180,0.039757)
mp59=(-0.071922,-0.023369,0.000000)
mp510=(-0.044450,-0.061180,0.000000)
mp910=(-0.052043,-0.037811,-0.039757)
mp94=(-0.071922,0.023369,0.000000)
mp95=(-0.071922,-0.023369,0.000000)
mp45=(-0.064329,0.000000,0.039757)
mp48=(-0.044450,0.061180,0.000000)
mp49=(-0.071922,0.023369,0.000000)
mp89=(-0.052043,0.037811,-0.039757)
mp83=(0.000000,0.075623,0.000000)
mp84=(-0.044450,0.061180,0.000000)
mp34=(-0.019879,0.061180,0.039757)
mp37=(0.044450,0.061180,0.000000)
mp38=(0.000000,0.075623,0.000000)
mp78=(0.019879,0.061180,-0.039757)
mp72=(0.071922,0.023369,0.000000)
mp73=(0.044450,0.061180,0.000000)
mp23=(0.052043,0.037811,0.039757)

fc123=(0.034695,0.025208,0.056138)
fc134=(-0.013252,0.040787,0.056138)
fc145=(-0.042886,0.000000,0.056138)
fc156=(-0.013252,-0.040787,0.056138)
fc162=(0.034695,-0.025208,0.056138)
fc1278=(0.013252,0.040787,-0.056138)
fc1289=(-0.034695,0.025208,-0.056138)
fc12910=(-0.034695,-0.025208,-0.056138)
fc121011=(0.013252,-0.040787,-0.056138)
fc12117=(0.042886,-0.000000,-0.056138)
fc723=(0.056138,0.040787,0.013252)
fc378=(0.021443,0.065994,-0.013252)
fc834=(-0.021443,0.065994,0.013252)

fc489=(-0.056138,0.040787,-0.013252)
fc945=(-0.069391,0.000000,0.013252)
fc5910=(-0.056138,-0.040787,-0.013252)
fc1056=(-0.021443,-0.065994,0.013252)
fc61011=(0.021443,-0.065994,-0.013252)
fc1126=(0.056138,-0.040787,0.013252)
fc2711=(0.069391,-0.000000,-0.013252)

disp_control = 0
P=101325.000000
d=-3.000000e+02

hollow_profile = 1
frame_beam_radius = 8.954073e-04
frame_beam_thickness = 4.477037e-05
frame_density = 1650.000000
frame_poisson = 0.200000
frame_modulus = 1.000000e+12
frame_seed_number = 18
frame_element_type = B32

skin_thickness = 7.280829e-06
skin_density = 1650.000000
skin_poisson = 0.200000
skin_modulus = 1.000000e+12
skin_seed_number = 18
skin_element_type1 = M3D3
skin_element_type2 = M3D3
skin_element_shape = TRI

skin_section_idealization = NO_IDEALIZATION
skin_section_location = MIDDLE_SURFACE
membrane = 1
no_stiffness_skin = 0

rays_select = 0
hollow_profile_rays = 1
rays_beam_radius = 0.000000e+00
rays_beam_thickness = 0.000000e+00
rays_density = 1650.000000
rays_poisson = 0.200000
rays_modulus = 1.000000e+12
rays_seed_number = 18
rays_element_type = B32

stiff_select = 0
hollow_profile_stiff = 1
stiff_beam_radius = 0.000000e+00
stiff_beam_thickness = 0.000000e+00
stiff_density = 1650.000000
stiff_poisson = 0.200000
stiff_modulus = 1.000000e+12
stiff_seed_number = 18
stiff_element_type = B32

```
rotations = OFF

model_name = 'icosahedron-Model'
job_name = 'icosahedron-Job'
job_name_odb = 'icosahedron-Job.odb'

# Step Information
buckle = 0
stabilization = 1
step_type = 0
nonlinear_effects = ON
increment_method = AUTOMATIC
stepname = 'Nonlinear-Static,General-wStabi'

# If Buckle
buck_num_Eigen = 5
buck_max_Iter = 30
buck_num_vectors = 30

# If General
initial_inc = 1.000000e+00
max_inc = 1.000000e+00
min_inc = 1.000000e-36
stabilization_ratio = 0.0500000000
stabilization_magn = 0.0002000000

# If Riks
initial_ArcInc = 1.000000e-01
min_ArcInc = 1.000000e-12
max_ArcInc = 1.000000e+00
maxnuminc = 100000000
max_LPF = 2.000000e+00

num_cores = 1
memory_usage = 1024
num_GPUs = 0
```

Bibliography

[1] Ardema, Mark D. Understanding NManualar Analysis. Report, Dassault Systemes SolidWorks Corp., 2008.

[2] Buckling analysis. [Online]. Availble: https://www.clear.rice.edu/mech403/HelpFiles/FEA_Buckling_analysis.pdf

[3] Century of Flight. Jules Henri Gi_ard (1825 - 1882), January 2014. URL [Online]. Available:
http://www.century-of-flight.net/Aviation%20history/to%20reality/Jules%20Henri%20Gi_ard.htm.

[4] Compression test. [Online]. Available: http://en.wikipedia.org/wiki/Compressive_strength

[5] Cranston, Brain (personal communication, June 2, 2015)

[6] Dassault Syste'mes. Abaqus Analysis User's Manual, 2011.

[7] Dassault Syste'mes, Providence, Rhode Island, 20010. Abaqus v.6.11.1.

[8] Davis, Tom. Lighter Than Air. The Johns Hopkins University Press, 2009.

[9] Glossary of Materials Testing. [Online]. Available: http://www.instron.us/wa/glossary/Compression-Test.aspx

[10] Grossman, Dan. Airships: The Hindenburg and other Zeppelins, January 2014. URL [Online]. Available: http://www.airships.net/dirigible.

[11] Lana-Terzi, Francesco. The Aerial Ship. The Aeronautical Society of Great Britain, 1910.

[12] M. W. Barclift, C. B. Williams, 2012, "Examining Variability in the Mechanical Properties of Parts Manufactured via Polyjet Direct 3D Printing," International Solid Freeform Fabrication Symposium, August 6-8, Austin, TX.

[13] Megan Hollander and Andrew Chalifoux. "Properties of Plastics And Their Applications to Rapid Prototyping" Boston University 2013. URL [Online]. Available: oned.bu.edu/me304/talk/5_2013.pptx

 [14] MTS, 2007. G200 nanoindenter manual. Document No. G2A-13192-0

[15] Newton's methods. Wikipedia URL [Online]. Available: http://en.wikipedia.org/wiki/Newton%27s_method.

[16] Palazotto, Anthony N. and Scott T. Dennis. NManualar Analysis of Shell Structures. American Institute of Aeronautics and Astronautics, 1992. ISBN 1-56347-033-0.

[17] PolyJet Materials Data Sheet. [Online]. Available: http://usglobalimages.stratasys.com/Main/Secure/Material%20Specs%20MS/PolyJet-Material-Specs/PolyJet_Materials_Data_Sheet.pdf?v=635376606224140355 [Accessed 04 June 2015].

[18] R. Adorno-Rodriguez, "Nonlinear Structural Analysis of an Icosahedron and its Application to Lighter than Air Vehicles Under a Vacuum," Air Force Institute of Technology, Wright-Patterson Air Force Base, Ohio, 2014.

[19] Saada, Adel S. Elasticity: Theory and Applications. J. Ross Publishing, Inc., 2nd edition, 2009. ISBN 978-1-60427-019-8.

[20] SolidWorks. [Online]. Available: http://en.wikipedia.org/wiki/SolidWorks

[21] Stratasys Launches Objet500 Connex3, World's First Multi-Material Color 3D Printer. [Online]. Availble: http://hothardware.com/news/stratasys-launches-objet500-connex3-worlds-first-multimaterial-color-3d-printer [Accessed 20 June 2015].

[22] T. T. Metlen, "Design of a Lighter than Air Vehicle that Achieves Positive Buoyancy in Air Using a Vacuum," Air Force Institute of Technology, Wright-Patterson Air Force Base, Ohio, 2013.

[23] The Origin of Icosahedral Symmetry in Viruses. URL [Online]. Available: http://virus.chem.ucla.edu/icosahedral_symmetry

[24] Wolfram MathWorld. Icosahedron, January 2014. URL [Online]. Available: http://mathworld.wolfram.com/Icosahedron.html.

[25] 3D printer. [Online]. Available: http://en.wikipedia.org/wiki/3D_printing

[26] 3D printing process. [Online]. Available: http://3dprintingindustry.com/3d-printing-basics-free-beginners-guide/processes

[27] Failure Criteria: Ductile Materials. [Online]. Available : http://www.efunda.com/formulae/solid_mechanics/failure_criteria/failure_criteria_ductile.cfm

[28] Pythagorean theorem. [Online]. Available: https://en.wikipedia.org/wiki/Pythagorean_theorem

REPORT DOCUMENTATION PAGE			*Form Approved* OMB No. 074-0188

The public reporting burden for this collection of information is estimated to average 1 hour per response, including the time for reviewing instructions, searching existing data sources, gathering and maintaining the data needed, and completing and reviewing the collection of information. Send comments regarding this burden estimate or any other aspect of the collection of information, including suggestions for reducing this burden to Department of Defense, Washington Headquarters Services, Directorate for Information Operations and Reports (0704-0188), 1215 Jefferson Davis Highway, Suite 1204, Arlington, VA 22202-4302. Respondents should be aware that notwithstanding any other provision of law, no person shall be subject to an penalty for failing to comply with a collection of information if it does not display a currently valid OMB control number.
PLEASE DO NOT RETURN YOUR FORM TO THE ABOVE ADDRESS.

1. REPORT DATE *(DD-MM-YYYY)* 17-09-2015	2. REPORT TYPE Master's Thesis	3. DATES COVERED *(From – To)* October 2013 – September 2015

TITLE AND SUBTITLE Finite Element Analysis and Experimentation of an Icosahedron Frame under Compression	5a. CONTRACT NUMBER
	5b. GRANT NUMBER
	5c. PROGRAM ELEMENT NUMBER
6. AUTHOR(S) AlGhofaily, Mohammed M., Captain, RSAF	5d. PROJECT NUMBER
	5e. TASK NUMBER
	5f. WORK UNIT NUMBER

7. PERFORMING ORGANIZATION NAMES(S) AND ADDRESS(S) Air Force Institute of Technology Graduate School of Engineering and Management (AFIT/ENY) 2950 Hobson Way, Building 640 WPAFB OH 45433-8865	8. PERFORMING ORGANIZATION REPORT NUMBER AFIT-ENY-15-S-051

9. SPONSORING/MONITORING AGENCY NAME(S) AND ADDRESS(ES) Air Force Institute of Technology Dr. Anthony Palazotto Graduate School of Engineering and Management (AFIT/ENY) 2950 Hobson Way, Building 640 WPAFB OH (937) 255-3636 x4599 anthony.palazotto@afit.edu	10. SPONSOR/MONITOR'S ACRONYM(S)
	11. SPONSOR/MONITOR'S REPORT NUMBER(S)

12. DISTRIBUTION/AVAILABILITY STATEMENT
 DISTRUBTION STATEMENT A**.** APPROVED FOR PUBLIC RELEASE; DISTRIBUTION UNLIMITED.

13. SUPPLEMENTARY NOTES
This material is declared a work of the U.S. Government and is not subject to copyright protection in the United States.

14. ABSTRACT

A nonlinear analysis of a 3D icosahedron frame was conducted using ABAQUS, under a compressive load in which collapse occurs. The frame was created in SolidWorks using the material properties of the 3D plastic building material VeroBlue. Two considerations were made: the computational features of the frame, and the comparison between the experimental solution to the numerical solution. Two studies were also considered in this research: The first study was a comparison between the seven-inch and the four-inch icosahedron model with identical weight to buoyancy ratios; and the second study was a comparison between the seven-inch icosahedrons frame, with the experimental results of the data that was collected. The results of both studies are analyzed to compare against and verify the results of numerical computational model.

15. SUBJECT TERMS
finite element analysis, modal analysis, structural analysis, lighter than air vehicles, icosahedron

16. SECURITY CLASSIFICATION OF:			17. LIMITATION OF ABSTRACT	18. NUMBER OF PAGES	19a. NAME OF RESPONSIBLE PERSON Dr. Anthony Palazotto, AFIT/ENY
a. REPORT	b. ABSTRACT	c. THIS PAGE	UU	88	19b. TELEPHONE NUMBER *(Include area code)* (937) 255-3636 x4599 anthony.palazotto@afit.edu
U	U	U			

Standard Form 298 (Rev. 8-98)
Prescribed by ANSI Std. Z39-18